The development of high-voltage measuring techniques

THE DEVELOPMENT OF HIGH-VOLTAGE MEASURING TECHNIQUES

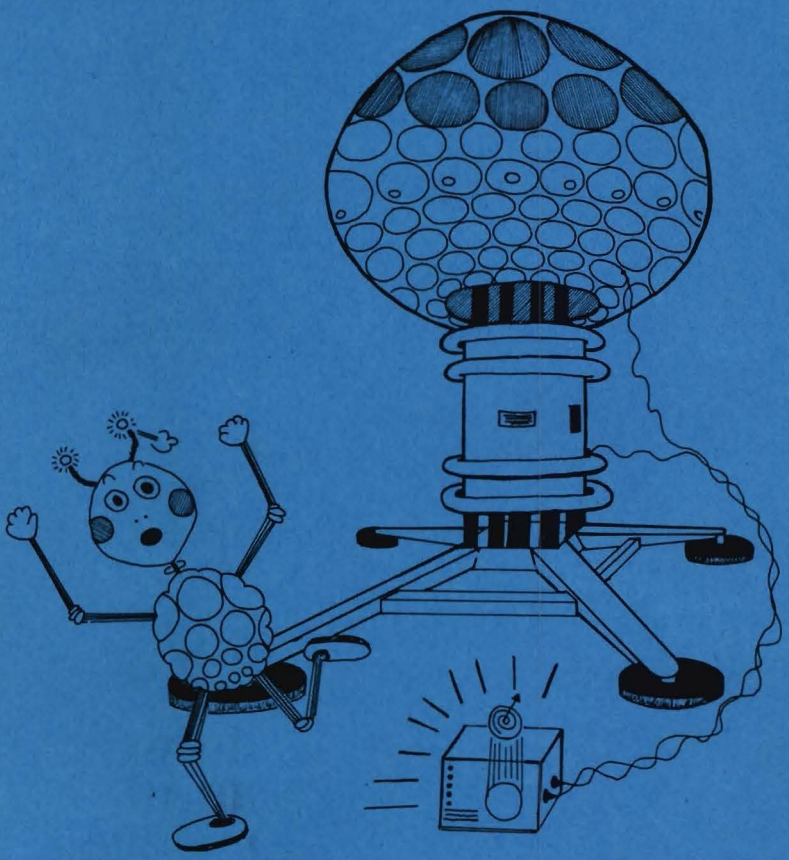

G.G. WOLZAK

THE DEVELOPMENT OF HIGH-VOLTAGE MEASURING TECHNIQUES

PROEFSCHRIFT

ter verkrijging van de graad van
doctor in de technische wetenschappen
aan de Technische Hogeschool Eindhoven,
op gezag van de rector magnificus,
prof.dr. S.T.M. Ackermans,
voor een commissie aangewezen door het
college van decanen
in het openbaar te verdedigen op
dinsdag 13 december 1983 te 16.00 uur.

door
Gerrit Gradus Wolzak
geboren te Oosterbeek

Dit proefschrift is goedgekeurd
door de promotoren:

Prof.dr.ir. P.C.T. van der Laan
en
Prof.Dr.-Ing. K. Möller

CIP-gegevens

Wolzak, Gerrit Gradus

The development of high voltage measuring techniques /
Gerrit Gradus Wolzak. - [S.l. : s.n.] - Fig. -
Proefschrift Eindhoven. - Met lit.opg., reg.
ISBN 90-9000549-8
SISO 661.1 UDC 621.317.32.027.3 UGI 650
Trefw.: hoogspanningstechniek / elektrische meettechniek.

Aan mijn ouders

Aan Annemiek

CONTENTS

* Paper published elsewhere

SUMMARY

This thesis describes developmental work on a number of high voltage measuring techniques. The emphasis of the development has been on measuring techniques for high voltages and on wide band partial discharge measurements.

Two methods have been developed for the measurement of high voltages, both with a single high voltage capacitor in the input circuit.
The first one - described in chapter 2 - is based on the consecutive differentiation and integration of the signal. An important advantage of this method is that a long measuring cable between the high voltage area and the measuring area can be included into the system without matching difficulties. Different measuring devices, based on this principle have been developed for dc, ac and impulse voltages; the results obtained with these devices are also reported in chapter 2.

The second method for voltage measurement is a modern version of a generating voltmeter. The voltmeter described in chapter 3 does not have a rotating electrode but a vibrating one, driven by a piezo electric transducer. The possibilities to use this device as a voltmeter and as a field meter are examined. The apparatus that was used to convert the modulated signal from the vibrating electrode into a signal proportional to the high voltage is briefly described; results obtained with one type of transducer are given.

Chapter 4 deals with the measurement of partial discharges in high voltages cables. A partial discharge caused by an imperfection in the cable insulation generates travelling waves between conductor and sheath. After a brief survey of the equivalent circuits for a partial discharge, the propagation of travelling waves in XLPE insulated high voltage cables is discussed. The attenuation of the travelling waves is mainly caused by the semiconducting layers on both sides of the insulation. The theoretical model is verified by attenuation measurements.

With the known properties of the cable, a theoretical model has been used to estimate the smallest partial discharge that can be detected. For a 30 m long cable of a given type the smallest detectable partial discharge turns out to be 0.05 pC. The travelling waves can be detected by two different methods: across an interruption of the cable sheath and by a coil wound around the sheath. The second method is only briefly dealt with here. The chapter concludes with some oscillograms of actually observed small partial discharges in different types of cables.

1. GENERAL INTRODUCTION

1.1. High-voltage measuring techniques

High-voltage technology has a wide range of applications. Large quantities of electrical energy are being transported today at voltages as high as 800 kV. Even higher voltages are achieved in electrostatic generators, in pulsed power machines (for particle beams and lasers) and in EMP simulators. These voltages may change in characteristic times ranging from hours (dc voltages) through milliseconds (50/60 Hz) to nanoseconds (impulse voltages).
Voltage measuring devices must be able to give an accurate reproduction of these signals at a level reduced to several (tens of) volts. They can be divided roughly into two categories: voltage transformers and dividers. Voltage transformers are used in every substation in the power distribution system, while voltage dividers are mainly used in laboratory measurements. The first half of this thesis deals with different voltage measuring systems with a single high voltage capacitor at the input.

Non-destructive tests of insulation quality is another important line of high voltage measurements. Two well known examples are the loss-tangent and the partial discharge measurements. The quality of an oil-paper dielectric can very well be estimated from the tan δ-voltage curve, which is a measure for the integral of the losses in the dielectric.
This method cannot be used for modern synthetic polymers such as epoxy resins and polyethene. These materials have a low loss-tangent but their insulating qualities suffer from the influence of small local imperfections, such as cavities. Partial discharge detection can "see" these individual faults; it offers a way to estimate the quality of the materials although the relationship between the partial discharges (pd) and long-term failure has not been firmly established. Chapter 4 of this thesis is devoted to partial discharge detection in high voltage cables. A wide band detection method is developed which allows

the detection and localization of very small partial discharges in relatively short cables.

Section 1.2 of this introduction gives some analogies between voltage and pd measurements, with special emphasis on the input circuits. The concluding section 1.3 gives a brief outline of the main experimental facilities which have been used in the investigations for this thesis.

1.2. Voltage measurements and partial discharge detection: analogies

A voltage measuring device measures a voltage at a well-defined point in a high-voltage circuit. Partial discharge measurements detect the fast voltage collapse across a void (of which the location is usually unknown) in a dielectric. Although these two measurements are different in several aspects, there are also a number of common features. Since these common features have been important in the developmental work, they are briefly surveyed here.

The importance of the input circuit. The correct definition, the frequency response and the wish to reduce the physical size of the input circuit are familiar problems in high voltage research, where the voltmeter leads are usually long. A well known example is the divider for high impulse voltage, where the connecting pipe can be several meters long. The main problem of long leads is the appreciable inductance; secundary problems for high frequencies are transit times and an incorrect impedance matching. Partial discharge measurements face a similar problem.
The collapse of the voltage across the tiny void has to reach the outside world through a voltage reduction across the whole sample. If the voltage drop across the whole sample is measured to obtain information on the process in the void, one can clearly speak of a voltmeter with poorly defined leads. As a result, the real voltage drop across the void is not measured but only the apparent charge.

A well-defined and compact input circuit in large objects can only be obtained in a number of special cases: partial discharge measurements in cables (coaxial geometry), built-in sensor in test objects (e.g. a divided electrode) etc.

Correct response over a wide frequency range is important for impulse voltage measurements but also for partial discharge measurements (improved sensitivity) and for any measurement where fast phenomena are being investigated. If the signal is not distorted by the input circuit itself, it still has to be transmitted to a measuring instrument of adequate bandwidth. The signal is usually transmitted over a long coaxial cable terminated with its characteristic impedance. This may look trivial, but as can be seen from numerous papers in the literature, it is not.

Transit times in large scale systems are inherent to the large size of the systems. This is true both for voltage and partial discharge measurements. Transit times are unavoidable; with a good experimental lay-out their influence can be partially reduced.

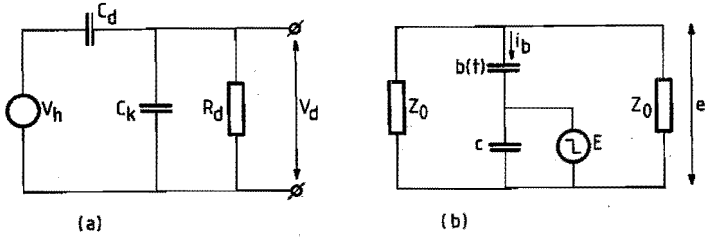

Figure 1.1. Analogy between voltage measurements and partial discharge measurements.
(a) Input circuit of a voltage measuring system
(b) Equivalent circuit for a partial discharge in a long cable.

An example of the similarity of voltage measurements and partial discharge measurements can be found by comparison of two figures in this thesis. The left part of Figure 2 in section 2.2 (reproduced as Figure 1.1a) shows the differentiating part of the voltage measuring system while the almost identical Figure 4.2 (reproduced as Figure 1.1b) shows an equivalent circuit for a partial discharge in a long high-voltage cable. Although the objectives are quite different, the equivalent circuits give a clear picture of the similarity in the approach of the measuring systems.

1.3. Experimental facilities

All experiments described in this thesis were carried out in the high-voltage laboratory of the Eindhoven University of Technology. The main dimensions of the shielded experimental enclosure are 24 x 18 x 14 m^3. The damping of radiated interference is 80 dB. The measuring apparatus can, whenever necessary, be located in a small screen room (2 x 1.5 x 2 m^3).

The ac experiments were carried out with a Hipotronics resonant test set. Only one of the three modules (300 kV, 2A each) was used. The clean waveform of the 50 Hz resonance gives a good suppression of conducted interference; this is especially important for partial discharge measurements. Impulse voltages were supplied by 5 stages of a 12 stage Haefely impulse voltage generator (200 kV, 2.5 kJ per stage).

A part of the experimental work for this thesis is described in three papers that were already published elsewhere. Two papers are co-authored by P.C.T. van der Laan who has initiated and stimulated this research. J.A.G. Bekkers, the other co-author of section 2.2 performed most of the experimental work reported in this section as a partial fulfilment of the requirements for a M.Sc. degree in Electrical Engineering.

2. VOLTAGE DIVIDERS WITH CONSECUTIVE DIFFERENTIATION AND INTEGRATION

2.1. Introduction

The measurement of high voltages generally involves the use of a voltage divider to bring the high voltage into a range that can be measured by a meter, oscilloscope or digitizer. Exceptions to this rule are the electrostatic voltmeter where the full voltage appears across the measuring capacitor and some optical voltage sensors, based on the Kerr- or Pockels effect.
The resistive divider is frequently used for the measurement of dc voltages. The electrostatic voltmeter and the generating voltmeter are also employed here. Measuring transformers are widely utilized for the measurement of ac voltages (e.g. in power distribution networks). In closed gas insulated systems (CGIS) the utilization of capacitive dividers is growing; these systems have a favorable geometry for a cylindrical high voltage capacitor. Impulse voltages (switching, lightning, EMP) are measured with capacitive, resistive and mixed dividers and with optical sensors.

Most dividers consist of two or more similar impedance elements to achieve - at least to a first approximation - a frequency independent dividing ratio. When the high voltage branch has a number of high voltage components, the parasitic impedances make it increasingly difficult to obtain a flat frequency response curve.

In this chapter a different type of divider will be described. The high voltage branch is a single capacitor of low value to avoid the problems with the parasitic impedances; the low voltage branch is a small measuring resistor. This divider has a ratio proportional to the frequency, in other words it acts as a differentiator. The low value measuring resistor can be formed by the characteristic impedance of a correctly terminated measuring cable; this cable can then be as long as the physical lay-out of the testing area requires, without any effect on the

dividing ratio.
To restore the shape of the original signal an integrator for the low voltage signal is necessary. Integration at the receiving end of a transmission line has the advantage that interference is also integrated, which means that an improved signal to noise ratio results. In fact the differentiator could be considered as a pre-emphasis network, analogous to the networks used in phonograph recording or FM-transmission.

The principle of consecutive differentiation and integration has been used in the past for fast pulse measurements in plasma physics experiments [Ke 64]. In the following three sections its use for dc, ac and impulse voltages is described.

Capacitive measurement of high dc voltages

G. G. Wolzak, J. A. G. Bekkers, and P. C. T. van der Laan

Eindhoven University of Technology, Department of Electrical Engineering, High Voltage Group, P.O. Box 513, 5600 MB Eindhoven, The Netherlands

(Received 20 April 1981; accepted for publication 3 July 1981)

This paper describes a new technique for the capacitive measurement of high dc voltages, based on the principle of consecutive differentiation and integration. A measuring electrode acts as the differentiating high-voltage capacitor; the electric flux to the measuring electrode can be intercepted by a movable shield. The signal is integrated with a commerically available integrator. The method has excellent accuracy and linearity, while the long-term stability is determined by the drift of the integrator. Calibration is only necessary after a change in the high-voltage circuit. The system is sensitive to corona, but the onset of corona can easily be observed by the operator. The described principle can also be used to measure 60 Hz and impulse voltages.

PACS numbers: 84.70. + p

INTRODUCTION

High voltages are usually measured with voltage dividers consisting of combinations of resistors, capacitors, and inductors. The high-voltage components of these dividers are large in size and therefore tend to have appreciable parasitic capacitances and inductances. When a number of high voltage components are used, the parasitic impedances make it increasingly difficult to obtain a flat frequency response curve.

These problems are largely avoided if the high-voltage branch of the divider consists of one single capacitor. Such a capacitor which could have air, SF_6, or oil as its dielectric can be a rather pure capacitive impedance. The other components of the divider are in the low-voltage branch and can be of normal size; because only low impedance values are needed in this branch, quite pure impedances are possible.

In the configuration of Fig. 1 the high-voltage capacitance, for instance, formed by a measuring electrode at some distance from a high-voltage object, carries a current

$$i = \frac{d}{dt}(CV_h) \quad \text{or} \quad i = \frac{d\psi}{dt}, \tag{1}$$

where Ψ is the electrical flux ending on the measuring electrode. Equation (1) shows that integration is required to obtain a voltage proportional to V_h; two methods are: (a) Z is a low-voltage capacitor. The divider is now a simple capacitive divider. The measuring instrument across the low-voltage capacitor should have a high impedance; (b) Z is a resistor. The RC combination differentiates, which means that a separate integrator is required. This principle, which was earlier employed by Keller[1,2] for fast pulse measurements, is used in this paper for measurements of dc voltages.

I. DIVIDER CIRCUIT

A circuit diagram of the measuring system is given in Fig. 2. The high-voltage capacitor is represented by C_d; in addition a capacitance C_k of the measuring electrode or the connecting cable to ground is shown. An operational amplifier with open-loop gain A is connected as an integrator. The following equations can be derived:

$$V_d = \frac{R_d R_i C_d}{R_d + R_i} \cdot \frac{dV_h}{dt}, \tag{2}$$

$$V_0 = \frac{1}{R_i C_i} \int_0^t V_d(\tau)\, d\tau = \frac{R_d C_d}{(R_d + R_i)C_i} V_h, \tag{3}$$

and are valid for the frequency range

$$\frac{1}{A(R_d + R_i)C_i} \ll \omega \ll \frac{R_d + R_i}{R_d R_i (C_d + C_k)}. \tag{4}$$

At low frequencies the integrator starts to fall off; at very high frequencies Eq. (2) fails because the parallel impedance of C_d and C_k is no longer large compared to the parallel resistance of R_d and R_i. Note that C_k has no influence on Eq. (2) when ω satisfies the inequality Eq. (4). Two limiting cases of the general Eq. (3) can be considered: (i) $R_d \ll R_i$. Eq. (3) now turns into

$$V_0 = \frac{R_d C_d}{R_i C_i} V_h. \tag{5}$$

In this case the differentiating part of the system acts as a voltage source for the integrator. An advantage is that R_d can be the matching resistor at the end of a long signal cable, so that the divider can have a flat response over a wide frequency range.[1] A disadvantage may be that the attenuation of the divider [Eq. (5)] can be too high.

(ii) $R_d \gg R_i$. Equation (3) now changes to

$$V_0 = \frac{C_d}{C_i} V_h, \tag{6}$$

where the assumption has been made that $AC_i \gg C_k$.

Here R_d can also be left out. Clearly the voltage V_h and the capacitor C_d act together as a current source for the integrator. In fact this case can also be described

 0034-6748/81/101572-03$00.60

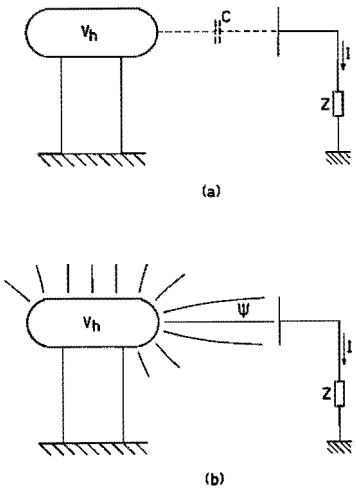

FIG. 1. Principle of the measuring system. (a) Capacitive divider scheme; (b) Electric flux pattern.

as a capacitive divider. The resistor R_i is not important anymore (see Eq. 6), although in practice R_i may protect the operational amplifier against large transients picked up by the connecting cable. The low-frequency limit of inequality (4) disappears, whereas the high frequency limit simplifies to $\omega \gg (R_i C_d)^{-1}$.

In the actual system a much more severe limitation will be that the nonterminated cable should remain much shorter than a quarter wavelength at any frequency in the signal to be measured.

At very low frequencies or for dc voltages a variation of C_d generates a signal according to Eq. (1), and simulates thereby a variation of V_h which can be more easily measured. The variation of C_d can be: (a) periodic as in generating voltmeters[3]; (b) caused by a motion of object and measuring electrode relative to each other[4]; (c) aperiodic, as in a situation where a grounded shield between object and electrode is removed. This last method is used in our measuring system.

II. APPARATUS

The measuring electrode is a 60° sector of a metal cylinder, insulated from the rest of the grounded cylinder

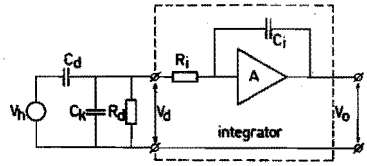

FIG. 2. Circuit diagram of the measuring system.

(see Fig. 3). No extreme insulation is required since the impedance level remains low. A second cylinder with an opening surrounds the first cylinder as a grounded shield. A remotely controlled electric motor inside the inner cylinder can turn the outer cylinder. In the "open" or measuring position the opening in the outer cylinder allows the measuring electrode to see the high-voltage object. In the "closed" position the measuring electrode is surrounded by the grounded outer cylinder. In this position the integrator can be reset. In view of the resemblance to a helmet with visor the system is named "the knight."

The signal of the measuring electrode is connected by a long coaxial RG 58/U cable to a stable integrator, the MI-3D integrator of Walker Magnemetrics.[5] This integrator has a 3½-digit display, a capacitor C_i of 10, 1 or 0.1 μF, and a resistor R_i which can be varied between 0 and 1 MΩ in steps of 100 Ω. The resistor R_d can be connected across the input of the integrator.

III. EXPERIMENTS

A. Linearity

The combination knight and integrator was tested in a simple corona-free setup with dc voltages up to 50 kV. The linearity of the system was checked against a resistive divider and an electrostatic voltmeter of 1% accuracy.

Figure 4 shows results for a number of values of C_d which was varied by changing the distance of the knight-high-voltage electrode (0.9 m for C_d = 0.35 pF).

B. Stability, influence of R_d, and drift

For a finite value of R_d, condition (4), $\omega A\ (R_d + R_i) \times C_i \gg 1$, is not satisfied at very low frequencies. In case

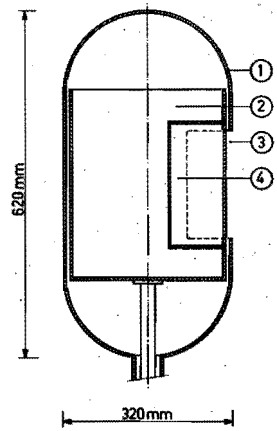

FIG. 3. The knight: (1) Outer cylinder; (2) Inner cylinder; (3) Opening in outer cylinder; (4) Measuring electrode.

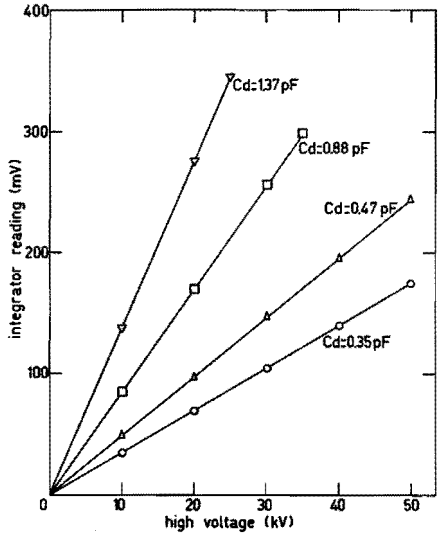

FIG. 4. Output signal of the integrator vs high voltage.

R_d is taken out, the left-hand side of condition (4) disappears, but then the drift of the integrator still limits the accuracy for long measuring periods. On the other hand, R_d cannot be chosen too low as this results in a too large attenuation of the signal [cf. Eq. (2)].

The open loop gain A of the integrator is 20,000. Condition (4) with $R_d = 500$ kΩ, $R_i = 50$ kΩ, and $C_i = 0.1\,\mu$F gives $\omega \gg 10^{-3}\text{s}^{-1}$, the corresponding period time $T \ll 100$ min!

However, the drift of the integrator is (after careful adjustment) in the order of 0.5%/min. This means, that the long-term stability of the system is determined by the drift of the integrator. Our experiments confirmed this fact. Therefore, all further measurements were carried out without R_d. The above stated drift of 0.5% per min provides enough time (typically several minutes) to read the display after opening the visor.

C. Corona

Corona in the high voltage circuit is a limitation to the accuracy of the system. This was verified by deliberately causing corona in the test setup. The corona impulses give a net current towards the electrode; this current is measured by the integrator. However, the fast rising output signal is a good indication for the onset of corona; an experienced operator can easily distinguish between corona-caused "drift" and the real drift of the integrator.

D. Calibration

We used an electrostatic voltmeter (accuracy 1%) to calibrate our system. Due to the good linearity calibration at one or two voltages is sufficient; there is no need for recalibration as long as the setup is not changed. It is also possible to calibrate the system with a 50- (or 60-) Hz ac voltage.

In a calibrated system expression (3) can be used to determine the value of C_d; if there is no standard voltmeter available, the measurement of C_d (with a capacitance bridge) and (3) can be used to calibrate the system.

ACKNOWLEDGMENT

The authors thank Th. G. van Moorsel who skillfully built the knight.

[1] R. Keller, Rev. Sci. Instrum. 35, 1057 (1964).
[2] C. A. Ekdahl, Rev. Sci. Instrum. 51, 1645 (1980).
[3] A. J. Schwab, *High Voltage Measurement Techniques* (MIT Press, Cambridge, 1971), p. 141.
[4] H. T. M. Haenen, J. Electrostatics 2, 203 (1976).
[5] The MI-3D integrator is almost identical to the MF-3D fluxmeter of Walker Magnemetics.

2.3. The measurement of ac (50 Hz) voltages with a differentiating/integrating divider

Voltage measurements in high voltage networks are important for protection and for monitoring the energy flow. Up till several years ago voltage measuring in networks was exclusively done with inductive voltage transformers. The increasing number of CGIS-stations and the modern protective circuitry have changed this fact.
In CGIS capacitive dividers can be used advantageously because the necessary high voltage capacitors can easily be built into the system. Secondly the power, required by the modern protective equipment has been reduced by two orders of magnitude [To 82], which makes the capacitive divider with its smaller power output more acceptable.

The possibilities for utilizing the differentiating/integrating divider as voltage monitor in substations are discussed in this section. The theory of the system is identical to the theory described in the sections 2.2 and 2.4. The special requirements concern the measurement of 50 Hz voltages with a low amplitude error (up to 0.1%) and a low phase error (down to 5'), which are necessary for the various categories of measuring systems in power engineering.
The accuracy is determined mainly by the high voltage capacitor. Small variations as a function of temperature or pressure (for a compressed gas capacitor) can lead to unacceptable errors. This is a matter of proper design of the hv capacitor; further details can be found in the literature [Gr 69] and will not be treated here.

The phase error requires a special design of the integrator. Generally an active integrator is used but as was shown in section 2.2 the drift in the output signal of an active integrator is a problem. For measurements in substations drift is, of course, unacceptable. This means that the working point of the integrator has to be stabilized for dc by means of an additional resistor R_2, see Figure 2.1. The output voltage V_o

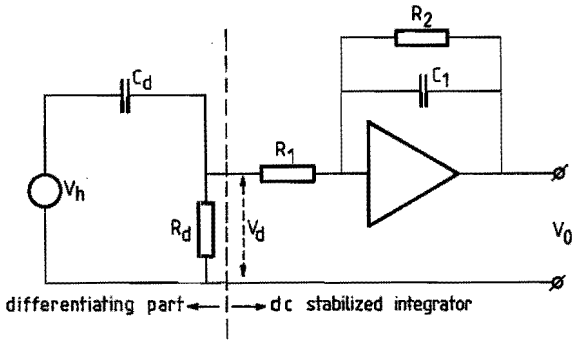

Figure 2.1 : Ac voltage divider with dc stabilized integrator.

is then given by:

$$V_o = -\frac{R_2}{R_1} \cdot \frac{1}{1 + j\omega R_2 C_i} V_d \qquad (2.1)$$

if the open loop gain A is high. The phase difference ϕ between V_o and V_d can be calculated from (2.1):

$$\phi = -\arctan(\omega R_2 C_i) \qquad (2.2)$$

For an ideal integrator ϕ equals $-\pi/2$; the phase error of the integrator from Figure 2.1 is therefore:

$$\Delta\phi = \arctan(\omega R_2 C_i) - \frac{\pi}{2} \qquad (2.3)$$

A phase error $\Delta\phi$ smaller than 5' at a frequency of 50 Hz is obtained for values of $R_2 C_i$ larger than 2.2 s. The phase error in the differentiating part is negligible; the differentiation of course introduces a phase shift of $\pi/2$.

Capacitive voltage monitors in CGIS can lead to a peculiar measuring problem, usually referred to as the "trapped charges problem" [IE 79]. If the circuit breakers of a transmission line open, some charge can be left on the line (and the divider).

If on subsequent reclosure these charges have not entirely decayed, while the output of the integrator has gone to zero (with a time constant R_2C_i) a dc error appears on the output, superimposed on the ac voltage. This error dies out with the same time constant R_2C_i, which is unacceptable for accurate measurements. It must be stressed however, that this phenomenon is inherent to all measuring systems which fail to correctly measure dc voltages. Inductive voltage transformers fail also in this respect but provide a dc path for the charges to leak away. If by some other means a dc leakage path is provided - as is anyway desirable to avoid dangerous overvoltages on CGIS - the capacitive voltage monitor will also function correctly.

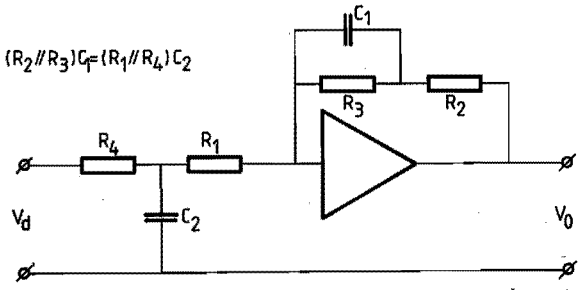

Figure 2.2 : Mixed passive/active integrator with improved pulse response.

If a measuring system is to be used to actuate protective circuitry, it must be able to give an accurate reproduction of transient signals. The rapidly changing high voltage causes a large current through the high voltage capacitor C_d in Figure 2.1. A part of this current goes through R_1 and therefore the operational amplifier must be able to supply as large a feedback current through C_i. This requires a carefully selected operational amplifier. In a modified integrator design, in which the passive integrator preceeds the active one the requirements on the operational amplifier are less stringent. Figure 2.2 gives an example of such a design. The choice of the components is governed by the condition:

$$\frac{R_2\ R_3}{R_2+R_3} \cdot C_1 = \frac{R_1\ R_4}{R_1+R_4} \cdot C_2 \qquad (2.4)$$

Some successful laboratory experiments at 50 Hz voltages were carried out with the coaxial high voltage capacitor ESPOM, described in the next section. Basically the measuring principle seems quite suitable for voltage monitors in substations. Extensive field tests and further work on the accuracy is however needed to convince potential users. Field tests will be carried out in the near future.

FOURTH
INTERNATIONAL SYMPOSIUM
ON HIGH VOLTAGE ENGINEERING
ATHENS - GREECE, 5 - 9 SEPTEMBER 1983

61.11

A NEW CONCEPT FOR IMPULSE VOLTAGE DIVIDERS.

G.G. Wolzak and P.C.T. van der Laan

Eindhoven University of Technology
Department of Electrical Engineering
Eindhoven, The Netherlands.

Abstract

In this paper we propose a new concept for impulse voltage dividers based on the principle of consecutive differentiation and integration of the signal. The high voltage element is a single gas-filled capacitor. This capacitor together with a long, characteristically terminated measuring cable which acts as a low value resistor, forms the differentiating part of the system. Integration is carried out by either a passive or an active integrator. We report measurements on standard (1.2/50 μs) pulses in addition the step response if the divider is measured according to the "sphere-gap" method. These measurements show the good transient behavior of the system. We discuss the most adequate type of integrator to be used and we pay attention to the shielding precautions, associated with the use of a "normal" oscilloscope for impulse voltage measurements.

Keywords

capacitor, divider, measurement.

1. Introduction: capacitive divider problems.

For the measurement of high impulse voltages, a voltage divider has to reduce the high voltage of up to some MV to a value that can be measured by an oscilloscope. For modern oscilloscopes this value is about 10-50 V. The low voltage signal must be a good reproduction of the rapidly changing high voltage. Three types of divider can be distinguished; resistive, capacitive and mixed dividers.
Resistive dividers with a low value of the total resistance (e.g. 10 kΩ) tend to load the high voltage circuit severely; high ohmic dividers suffer from the influence of stray capacitances. Mixed dividers, having resistors and capacitors either in series or in parallel are used in many laboratories but tend to be rather complex and pose a linearity problem. The advantages of a single capacitance in the high voltage circuit have been described previously. This capacitance can be a compressed gas capacitor [1] or be formed by an electrode at some distance of a high voltage object [2]. Also the use of a coaxial tubular capacitor for testing metal enclosed switchgear has been reported [3].
The problems, associated with the use of undamped capacitive dividers can be summarized as follows:

a) Natural frequencies of the low voltage arm. Special care has to be taken to ensure a very low inductance of the low voltage arm. Usually special capacitors [4] or a number of capacitors in parallel [5] are emloyed.
b) Travelling wave oscillations on the transmission line between the high- and the low-voltage arm. These oscillations occur when a compressed gas capacitor is used [1].
c) The matching of the signal cable which cannot be properly terminated with its characteristic impedance. To prevent multiple reflections, a series resistor is often employed.

2. The new approach.

2.1. Principle.

The divider we propose is based on the principle of consecutive differentiation and integration of the signal [2,6,7]. The differentiating part of the divider is a single high voltage capacitor, connected to a long terminated measuring cable which acts as a low value resistor, Figure 1.

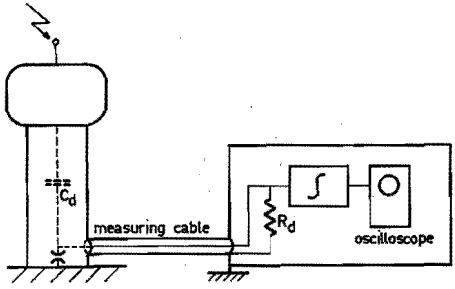

Figure 1. Principle of the new divider.

The integrator, either passive or active, and the oscilloscope are in a shielded measuring room. The circuit diagram of the measuring system is given in Figure 2. The high voltage capacitor is presented by C_d, the parasitic capacitance is given by C_k. If $R_i \gg R_d$ the following equations can be derived:

$$V_d = R_d C_d \frac{dV_h}{dt} \qquad (1)$$

$$V_o = \frac{1}{R_i C_i} \int_0^t V_d(\tau)d\tau = \frac{R_d C_d}{R_i C_i} \cdot V_h \qquad (2)$$

(1) and (2) are valid for the frequency range:

$$\frac{1}{R_i C_i} \ll \omega \ll \frac{1}{R_d(C_d+C_k)} \qquad (3)$$

If an active integrator with open loop gain A is used (Figure 2b) the lower frequency limit becomes

$$(AR_iC_i)^{-1}$$

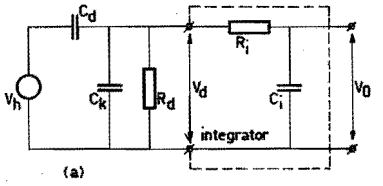

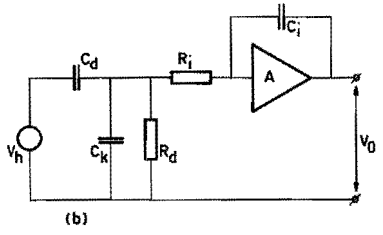

Figure 2. Equivalent circuit of the measuring system
a. with passive integrator
b. with active integrator

Equation (2) gives the ratio of the divider. The product R_iC_i is determined by the length of the pulse to be measured (see 2.3) and cannot be chosen too small ($R_iC_i = 10^{-5} - 10^{-3}$ s). R_d is generally 50 ohm and C_d is 10 - 100 pF. This means that the divider ratio (the attenuation of the signal) will be in the order of 10^5 to 10^7.

2.2. Inductance in the high voltage circuit.

The impulse generator and the divider are connected by a high voltage lead. The inductance of this lead (and the inductance of the grounding circuit) cannot be neglected. In Figure 3 the modified equivalent circuit for the differentiating part is given.

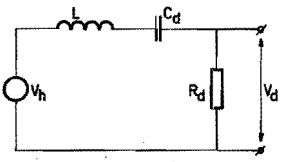

Figure 3. Modified equivalent circuit.

We can now derive:

$$\frac{V_d}{V_h} = \frac{j\omega R_d C_d}{-\frac{\omega^2}{\omega_o^2} + \frac{j\omega Q}{\omega_o} + 1} \qquad (4)$$

$$\text{With } Q = \frac{\sqrt{L/C_d}}{R_d} \quad \text{and} \quad \omega_o^2 = \frac{1}{LC_d} \qquad (5)$$

We can see that the inductance L influences the upper limit of the frequency range, specified in (3). Very small inductances would in fact improve the frequency response; a series L-C-R circuit with $Q = \frac{1}{2}\sqrt{2}$ has a more linear response than a C-R circuit without L. For typical values, C_d = 10 pF and R_d = 50Ω this optimal value is 12.5 nH, which is much smaller than the values of several μH to be expected in a practical situation. The upper frequency limit of (3) is therefore lowered to approximately the ω_o of (5). An extra damping resistor at the high voltage side is required to avoid a resonance peak.
This problem always has to be faced when a test-object is connected with several meters of high voltage lead. If the capacitor can be built into the test set-up (e.g. in CGIS) the inductance in the high voltage circuit does influence the test voltage waveform and the measurement simultaneously. In that case a true representation of the test voltage is obtained.

2.3. Integration.

Three types of integrators were considered for the new measuring system, see Figure 4. The passive RC integrator has the advantage of being very simple, but its application is limited due to droop problems. When we want to measure a full 1.2/50 μs impulse with an accuracy of 5% we have to choose $RC \geq 2$ msec. This means a very large attenuation of the signal, according to (2).

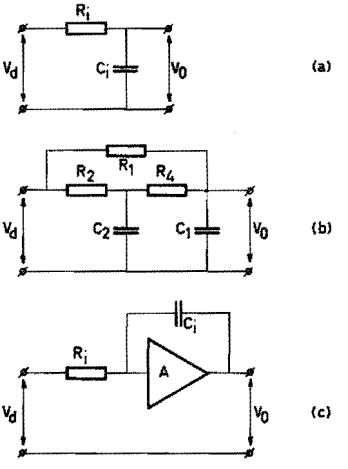

Figure 4. Different types of integrators.
a. passive
b. passive, compensated
c. active, Miller.

The compensated passive integrator [8] shows a much better droop behavior. A two stage compensated integrator (Figure 4.b) with $R_iC_i \approx 2$ msec can measure a 1.2/50 μs pulse with a droop of ≤ 1%. Three or four stage compensated integrators behave even better. However, one still has to choose the product R_iC_i equal to about ten times the pulse length.
The active Miller integrator shows the best behaviour at low frequencies. Compared with a passive integrator the RC time can be a factor A (the open loop gain) smaller to obtain the same low frequency cut-off. However, when measuring steep pulses (like chopped impulse voltages) the opamp must be able to supply the required current in C_i. This requires a careful selected opamp.

3. Apparatus.

For our experiments we used a coaxial high voltage capacitor, ESPOM, a part of a metal enclosed SF_6-insulated switchgear installation; a simplified view is given in Figure 5. The measuring capacitance C_d

is 10 pF; the total capacitance, including the bushing is 134 pF.
Special attention is paid to the differentiating resistor R_d. When the high voltage changes rapidly (e.g. is chopped), the current through R_d can be high (> 100 A), as can be seen from (1). Therefore R_d is constructed from 20 low-inductance resistors - each 1 kΩ, 1 W - in parallel.

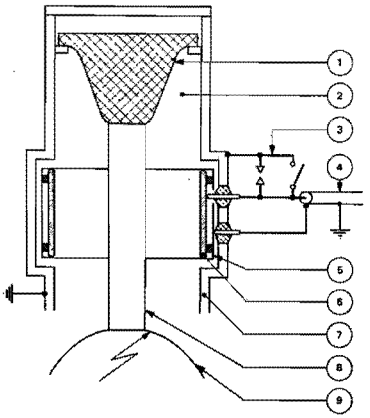

Figure 5. Coaxial high voltage capacitor ESPOM.

1. epoxy-resin support
2. gaseous dielectric
3. surge arrestor + earthing switch
4. shielded cable
5. earth screen
6. measuring electrode
7. enclosure (pressure vessel)
8. centre electrode
9. HV-connection.

The differentiating resistor R_d, the integrator and the oscilloscope (Tektronix type 7844) are placed in a small shielded room. The low voltage terminal of the capacitor and R_d are connected by a 16 m long RG 214/U cable in a copper pipe. The pipe and the cable shield are grounded at the entrance of the shielded room and at the enclosure of the capacitor. To maintain shielding integrity a small brass box surrounds the short open leads near the ESPOM connections.

4. Experiments.

4.1. Measurement of full impulse voltages.

To avoid droop problems in measurements on especially the tail of full impulse voltages we used an active integrator with R_i = 100 kΩ, C_i = 100 pF and open loop gain A = -2500. These values set the ratio of the divider to $2 * 10^4$.
Figure 6 shows an oscillogram of a 200 kV impulse. The front of the impulse shows a "clear" picture (no oscillations occur), indicating the adequate shielding against interference.

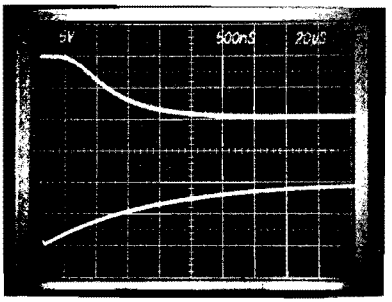

Figure 6. Full (1.2/50 μs) impulse voltage.

4.2. Measurement of the step response.

The large ratio of the divider makes it impossible to use a mercury wetted relay for the measurement of the step response. The alternative is the "sphere gap method" [9] which also had the advantage that the system is tested at more realistic values of the voltage and dV/dt.

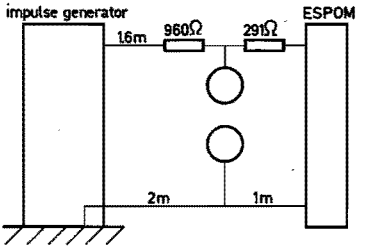

Figure 7. Test set-up for impulse response measurement.

Figure 7 shows the test set-up; the two damping resistors are needed to prevent oscillations in the high voltage circuit. All the connections (high voltage and ground) are made with brass pipes, of 42 mm diameter. The spheres have a diameter of 20 cm, the distance between the spheres is 4 cm. A measured step response is given in Figure 8. We could use a passive integrator here (10 kΩ, 10 nF) because the emphasis is not on the tail of the impulse. The rise time of the signal (10-90%) is 120 ns, the overshoot is small, 5%. Computer calculations, in which we took into account the total capacitance of the ESPOM, the inductance of high-voltage and grounding leads and the resistors in the circuit, show that the risetime and the overshoot are determined by these components. This means that the actual response of the divider may even be faster, but cannot be ascertained in this way.

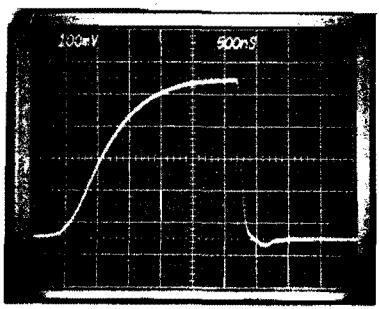

Figure 8. Step response oscillogram.

5. Conclusion.

The advantages of a single capacitor as primary element in an impulse voltage divider are fully exploited when this capacitor forms a part of a differentiating-integrating meauring system: no travelling wave between high and low voltage arm and an easy matching of the measuring cable. The experiments have shown a good step response. The integrator has to be chosen carefully.

6. Acknowledgement.

The authors thank COQ in Amersfoort, The Netherlands who put the ESPOM-system at their disposal. They also like to thank Th.G.M. van Moorsel for his technical assistance during the measurements.

7. References.

[1] Schwab, A.J., Pagel, J.E.: "Precision capacitive voltage divider for impulse voltage measurements". IEE Transactions vol. PAS 91 (1972) pp 2376-2382.

[2] Wolzak, G.G., Bekkers, J.A.G., van der Laan, P.C.T.: "Capacitive measurement of high dc voltages". Rev.Sci.Instrum. vol. 52 (1981) pp 1572-1574.

[3] Breilmann, W.: "Effects of the leads on the transient behaviour of a coaxial divider for the measurement of high alternating and impulse voltages". 3rd International Symposium on High Voltage Engineering, Milan, Italy, 28-31 August 1979, Paper 42.12.

[4] Harada, T., Aoshima, Y.: "Development of high performance low voltage arms for capacitive voltage divider". 3rd International Symposium on High Voltage Engineering, Milan, Italy, 28-31 August 1979, Paper 42.14.

[5] Schwab, A.J.: "High Voltage Measurement Techniques". MIT Press, Cambridge, 1971.

[6] Keller, R.: "Wideband high voltage probe". Rev.Sci.Instrum. vol.35 (1964), pp 1057-1060.

[7] Ekdahl, C.A.: "Voltage and current sensors for a high-density z-pinch experiment". Rev.Sci.Instrum. vol.51 (1980), pp 1645-1648.

[8] Cross, R.C., Collins, G.A.: "Compensated RC integrators". Am.Journal of Physics, vol.49 (1981) pp 479-480.

[9] CIGRE Working Group 33.03: "Record of performace of voltage and current measuring systems". Electra, no. 78 (1981) pp 35-69.

3. A GENERATING VOLTMETER WITH PIEZO ELECTRIC MODULATION

3.1. Introduction

Generating voltmeters were originally developed as non-contacting dc voltmeters or fieldmeters. Their common aspect is a mechanically modulated measuring electrode, capacitively coupled to the test object (or test field). The modulation generates an ac signal, proportional to the voltage difference between electrode the high voltage object.
Three basic modulation techniques can be distinguished [Vo 74]:
- the rotating segmented disc (field mill),
- the oscillating vane (tuning fork),
- the vibrating capacitor.

All three principles have been developed into commercially available instruments. The vibrating capacitor technique was first described by Zisman [Zi 32], who used a piano wire to drive an electrode. Later versions of Gohlke and Neubert [Go 40] and van Nie and Zaalberg [Ni 63] use a coil and a membrane capacitor respectively.

In this chapter the possibilities of a vibrating capacitor driven by a piezo electric crystal will be examined. The use of a piezo transducer has two advantages:
- the vibration frequency can be significantly higher than the frequency obtained with other transducers. This opens the possibility to widen the frequency range of the high voltage to be measured. Whereas for instance the field mill can only be used to measure dc voltages, an extension to at least power frequencies (50 or 60 Hz) is very interesting.
- The reliability of a transducer is much higher than that of the other techniques, because mechanical wear is no longer important.

A possible problem is the small amplitude of the vibration (a few μm), which will lead to very small signals.

3.2. Theory

Consider the capacitor of Figure 3.1. The distance between the high voltage electrode and the central low voltage (measuring) electrode varies as a function of time according to:

$$d(t) = d_o + \hat{d} \sin \omega_k t \tag{3.1}$$

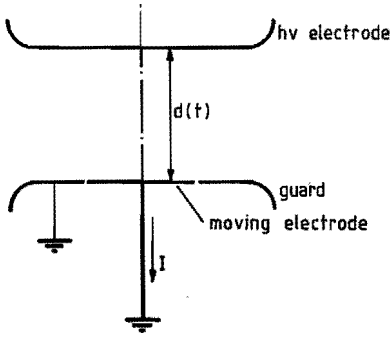

Figure 3.1 : Principle of vibrating plate capacitor.

If the measuring electrode has an area A and (3.1) is substituted in the expression for a parallel plate capacitor, the capacitance C(t) is given by:

$$C(t) = C_o + \Delta C \sin \omega_k t \approx \frac{\varepsilon_o A}{d_o} \left(1 - \frac{\hat{d}}{d_o} \sin \omega_k t\right) \tag{3.2}$$

The displacement current I flowing from the measuring electrode to ground can then be calculated:

$$I(t) = \frac{d}{dt} (CV_h) = C \frac{dV_h}{dt} + V_h \frac{dC}{dt} \tag{3.3}$$

Two cases can be distinguished:

A. The voltage V_h is a dc voltage: $dV_h/dt = 0$.
Eq. (3.3) turns into a very simple expression:

$$I(t) = V_h \frac{dC}{dt} \tag{3.4}$$

Combination of (3.4) with (3.2) gives:

$$I(t) = - V_h \omega_k \frac{\hat{d}}{d_o} C_o \cos \omega_k t \tag{3.5}$$

C_o was already defined as

$$C_o = \frac{\varepsilon_o A}{d_o} \tag{3.6}$$

The current I is a sinewave with an amplitude proportional to the high voltage V_h, see Figure 3.2.

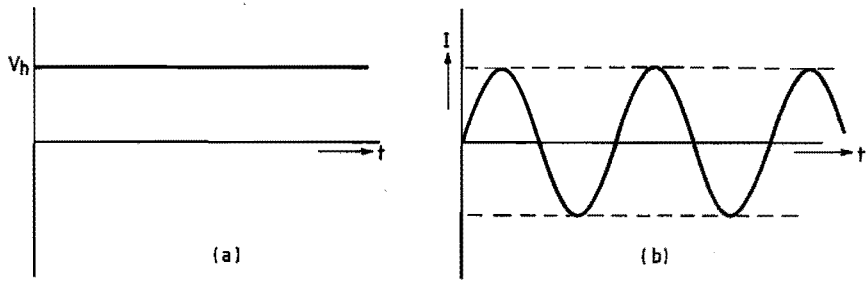

Figure 3.2 : The input voltage (a) and the output current (b) for a high dc voltage.

B. The voltage V_h is an ac voltage:

$$V_h(t) = \hat{V}_h \sin(\omega_h t + \phi) \tag{3.7}$$

where $\omega_h << \omega_k$.
The current I has two components, according to (3.3):

$$I_1(t) = C(t)\,\frac{dV_h}{dt} \approx C_o\,\omega_h\,\hat{V}_h\,\cos(\omega_h t + \phi) \qquad (3.8)$$

$$I_2(t) = V_h(t)\,\frac{dC}{dt} = -\,\hat{V}_h\,\omega_k\,\Delta C\,\sin(\omega_h t + \phi)\,\cos(\omega_k t) \qquad (3.9)$$

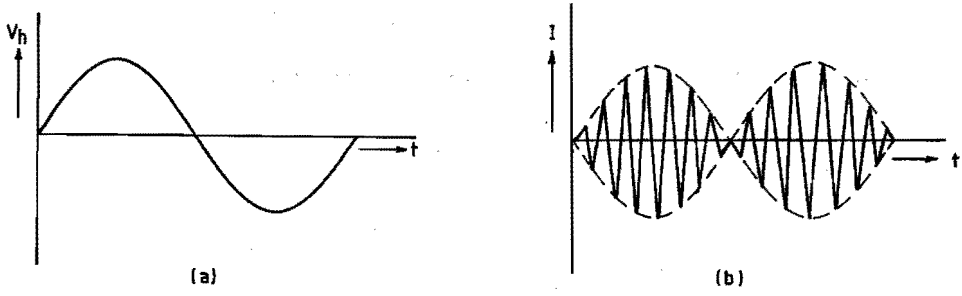

Figure 3.3 : The input voltage (a) and the output current (b) for a high ac voltage.

The first component I_1 represents the 'normal' displacement current and is independent of the movement of the electrode. The current I_2 is a modulated ac current, see Figure 3.3. The type of modulation is known as double sideband suppressed carrier (DSSC) modulation [Ca 75]. The frequency spectrum of I_1 and I_2 is given in Figure 3.4.

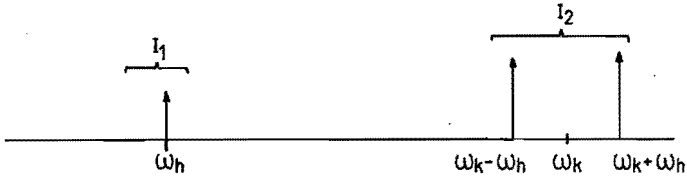

Figure 3.4 : Frequency spectrum of the output current (I_1 + I_2) for a high ac voltage.

The currents, described by (3.5) and (3.9) have to be measured and demodulated to obtain a signal proportional to the voltage

$V_h(t)$. The details of the current measurement and demodulation are treated in the next section. From (3.5) and (3.9) another important fact can be learned: both expressions show a $\Delta d/d$-dependence in the current I.
This means that the current becomes very small for a remote high voltage source: the device cannot be used as a field meter. However, the movement of the central electrode in an electrical field causes an additional effect which is independent of distance.

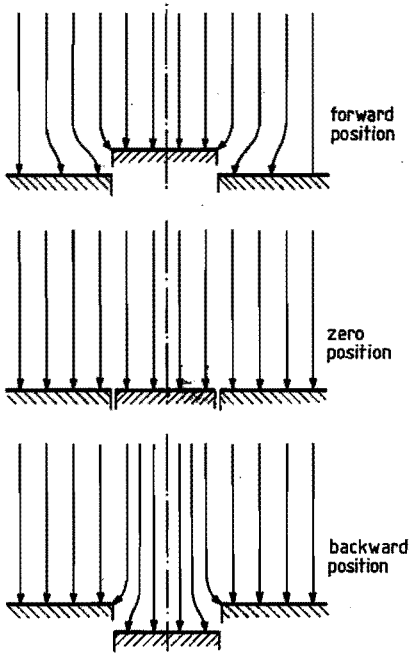

Figure 3.5 : Field pattern for the different positions of the measuring electrode.

The movement of the measuring electrode causes not only a change in the length of field lines but also a change in the electric field pattern. This can be seen from Figure 3.5 where the field lines are sketched for three positions of the measuring electrode.

The variation in the number of field lines is equivalent to a time varying flux, in other words to a small current.
An exact calculation of the amplitude $\Delta\psi$ of this flux change requires a detailed knowledge of the electric fieldstrength along the electrode. This problem can be solved by conformal mapping for a two dimensional situation [Be 63] but this solution gives a diverging value for $\Delta\psi$ at large distances from the high-voltage electrode. For an electrode in the form of a half sphere, the flux to the half sphere is $3\pi r^2\varepsilon_o E_o$ [Pr 69], where r is the radius of the sphere. Compared to the flux to the plane, when the half sphere has flattened out this corresponds to $\Delta\psi = 2\pi r^2\varepsilon_o E_o$.
For a vibrating circular electrode of radius r in a plane a first order approximation is adopted here.

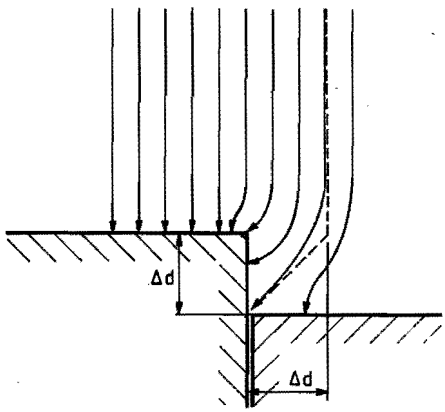

Figure 3.6 : Extension of the field disturbance in the extreme position of the electrode.

If the field pattern of Figure 3.6 is assumed for the forward position of the measuring electrode then additional flux coming from a radius r + Δr is seen to end on it. The additional flux is limited by the field line which ends in the lower corner. Since this field line leaves under 45^o it is reasonable to assume that $\Delta r \approx \hat{d}$. The extra flux $\Delta\psi$ is then:

$$\Delta\psi = \varepsilon_o E_o 2\pi r \hat{d} \tag{3.10}$$

In the extreme downward position the total flux to the measuring electrode is diminished by $\Delta\psi$.
If the movement of the electrode is given by (3.1), the current generated by this variation in the flux is:

$$I_3(t) = \frac{d}{dt}(\Delta\psi) = \varepsilon_o E_o \omega_k 2\pi r \hat{d}\cos\omega_k t \tag{3.11}$$

This expression is similar to (3.5): a time independent field E_o is assumed. For a time dependent field expressions comparable to (3.8) and (3.9) are obtained. The next question is: what is the relative importance of these two effects?
The ratio of I/I_3 can be calculated from (3.5) and (3.11):

$$\frac{I}{I_3} = \frac{r}{2d_o} \tag{3.12}$$

The currents are equal for $r = 2d_o$; for larger distances the I_3 component is dominant.

3.3. Apparatus

In this section the different components of the generating voltmeter system will be treated. The realization of the vibrating electrode will be described first. Then attention is paid to the current measuring system, consisting of a Rogowski coil and a lock-in amplifier, which also acts as a demodulator for the signals.

The measuring electrode

The design of the test set up with a vibrating measuring electrode is based upon two important considerations:
- efficient coupling between the piezo-electric crystal and the electrode,
- the exciter signal of the crystal must remain decoupled from the current to be measured.

The approach to fulfill these requirements is sketched in Figure 3.7.

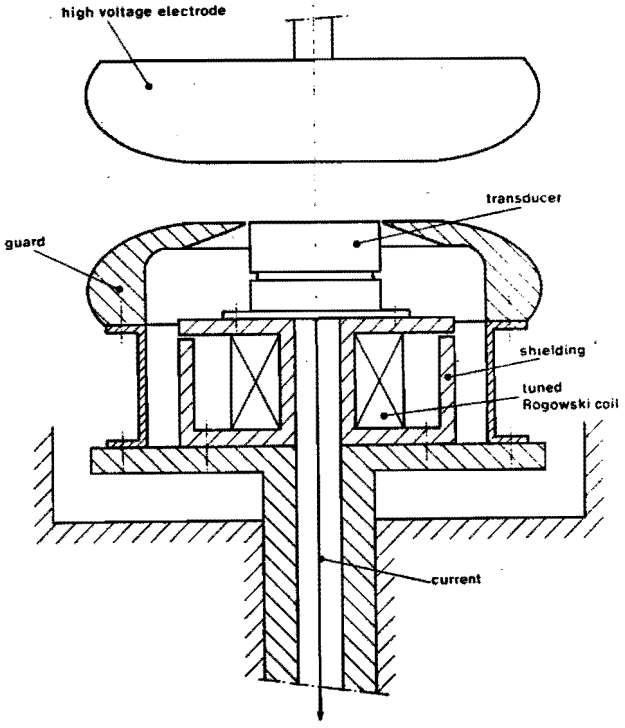

Figure 3.7 : The test set-up with the Sonair transducer.

The vibrating front plane of a commercially available transducer (Sonair 2 from Vernitron Ltd) serves as a measuring electrode. The aluminum housing of the transducer gives a good shielding against the excitation signal of the crystal. Figure 3.7 also illustrates why the measurement of the displacement current requires special care: a small current is superimposed on the much larger excitation current of the transducer. The use of a Rogowski coil is ideal here: the current for the transducer is fed through a coaxial cable and the measuring

current goes through the sheath of the cable. The Rogowski coil only "sees" the net current. Further details of the coil will be given later in this section.
The transducer (28 mm diameter) is placed in the center of an aluminum Rogowski-profiled electrode (15 cm diameter). The high voltage electrode is identical in shape. The system operates at a frequency of 40 kHz, the estimated amplitude of the vibration is in the order of .1 μm.

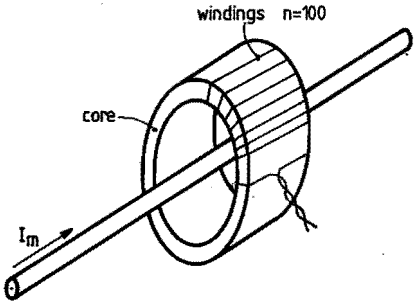

Figure 3.8 : Principle of the Rogowski coil.

The Rogowski coil and lock-in amplifier

The simplest way of current detection is usually the measurement of the voltage drop over a series resistor. However, a series resistor cannot be used with the Vernitron transducer while application with the HPA transducer is somewhat difficult. Furthermore a resistor implies galvanic coupling between the sensitive measuring circuitry and the high voltage circuit; this can be disastrous in the case of a breakdown or flashover. A Rogowski coil offers a good solution but the transfer impedance, defined as the ratio of output voltage and input current must be as high as possible.
Figure 3.8 gives a picture of the coil and Figure 3.9 a simple equivalent circuit. The mutual inductance can be calculated with:

$$M = n \frac{\mu_o \mu_r h}{2\pi} \ln \frac{r_2}{r_1} \qquad (3.13)$$

where n is the number of turns, h is the height of the coil; r_2 and r_1 are the outer and inner radius respectively. If in Figure 3.9: $R_2 >> \omega_k L_2$ and $C_2 << 1/\omega_k^2 L_2$ the output voltage V_2 is given by:

$$V_2 = \omega_k M I_1 \qquad (3.14)$$

The number of ways to increase the value of M is limited:
- the dimensions of the coil cannot be too large,
- a ferrite core with a high value of μ_r can be used,
- the number of turns n is limited.

In this case, ferrite cores (r_1 = 11 mm, r_2 = 18 mm, μ_r = 3000) were used. The height h was increased by stacking two cores. On the cores were 100 turns of .2 mm copper wire. The value of M, according to (3.13) is then 0.8 mH.
The output voltage V_2 can be further increased by tuning the Rogowski coil. The choice of the capacitor C_2 in Figure 3.9 should then be such that the condition

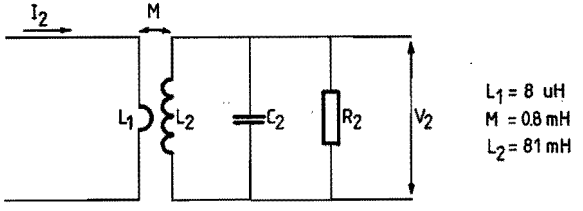

Figure 3.9 : Simplified equivalent circuit for the Rogowski coil.

$$\omega_k L_2 = \frac{1}{\omega_k C_2} \qquad (3.15)$$

is fulfilled. The capacitance C_2 is composed of:

- the capacitance of the cable to the voltmeter,
- the input capacitance of the voltmeter,
- the tuning capacitance.

The output voltage of the tuned Rogowski coil is given by:

$$V_2 = Q\ \omega_k\ M\ I_1 \tag{3.16}$$

where Q is the quality factor of the secondary circuit:

$$Q = R_2 \sqrt{\frac{C_2}{L_2}} \tag{3.17}$$

The value of R_2 (the input resistance of the voltmeter) can be chosen high (e.g. 100 MΩ) to increase Q. In practice, however, Q is limited by the losses in C_2, L_2 etc. A practical value for Q, also confirmed by a number of measurements is: Q = 30.
It must be stressed that the tuned coil has a strong frequency selective behavior. This is normally considered as a disadvantage for a wideband measuring system but it is a big advantage for a carrier based system like this. From (3.17) a transfer impedance can be derived:

$$R_t = \frac{V_2}{I_1} = Q\ \omega_k\ M \tag{3.18}$$

The value of R_t gives the apparent measuring resistance, seen from the voltmeter's side. For this situation a value for R_t of 6 kΩ can be calculated. The high voltage circuit "sees" in the ground lead only an impedance of $Q\ \omega_k\ L_1$ (= 60 Ω).

This section concludes with a basic description of the lock-in amplifier. A lock-in amplifier is an ac voltmeter, which is able to measure the amplitude of a signal of known frequency in the presence of high level background noise or interference. Basically a lock-in amplifier is a phase sensitive ac voltmeter which compares an input signal with a reference to produce a dc signal output whose level is proportional to that part of the signal synchronous and in phase with the reference.

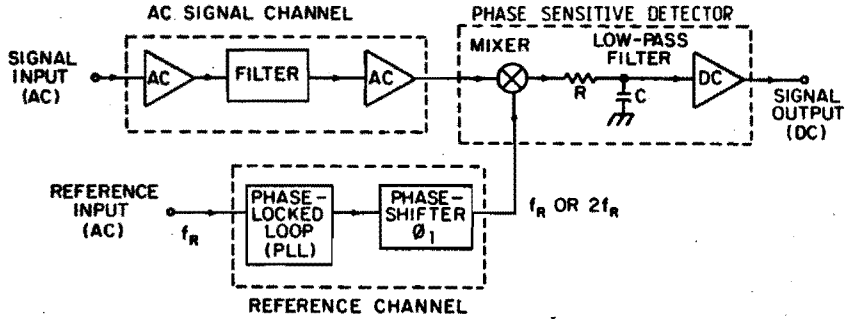

Figure 3.10 : Block diagram of the lock-in amplifier.

A block diagram of the lock-in amplifier is given in Figure 3.10. Three basic blocks can be distinguished: the ac signal channel, the phase sensitive detector and the reference channel. In the signal channel, the input signal (and noise) is conditioned by a low-noise preamplifier and a second amplifier, with an in-between filter. This predetection filter can be a tunable bandpass, notch, low-pass or high-pass network; it reduces the noise and thus the possibility of overloading the mixer.

The reference channel transforms an externally applied reference to a suitable square wave (at the reference frequency) to drive the mixer.

The phase sensitive detector, the combination of mixer, low-pass filter and dc amplifier produces a dc voltage, depending on the phase difference between the signal and the reference. The results, reported in the next section were obtained with a Princeton Applied Research (PAR) lock-in amplifier which has the following characteristics:

- sensitivity: 1 μV to 250 mV full scale,
- frequency range: 0.5 Hz - 100 kHz,
- input impedance: 100 MΩ in parallel with 20 pF.

3.4. Experiments; discussion

The system with the Sonair 2 transducer (see Figure 3.7) was tested with dc voltages up to 30 kV and 50 Hz ac voltages up to 20 kV rms. The output voltage of the lock-in amplifier was compared to a direct high voltage measurement with a Singer electrostatic voltmeter (error 1%).

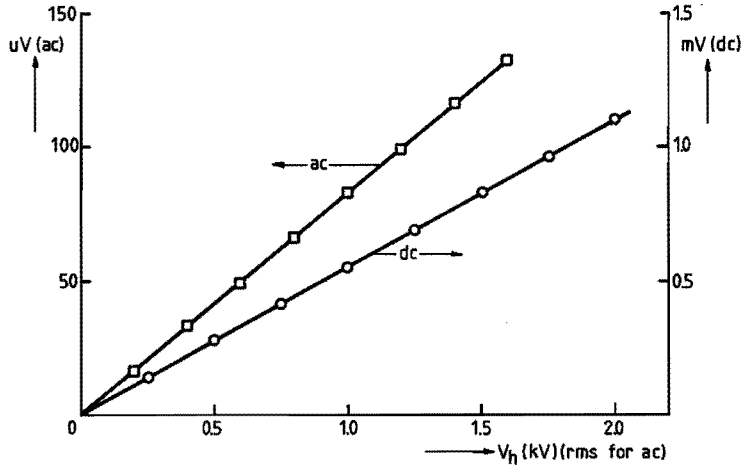

Figure 3.11 : Output voltage of the lock-in amplifier versus high-voltage. Test set-up with the Sonair transducer.

Figure 3.11 gives a picture of the linearity of the system. The distance between the electrodes was 1 mm in these experiments. The linearity is very good, both for dc and ac. The measured signal is roughly a factor 10 smaller with ac voltages. This is caused by a low-pass filter in the lock-in amplifier (time constant 10 ms, 6 dB/octave) which gives a 10 dB damping for 50 Hz signals. This filter was built in the lock-in amplifier and could not be switched off: for a 50 Hz measuring system a more appropriate filter would have to be constructed.

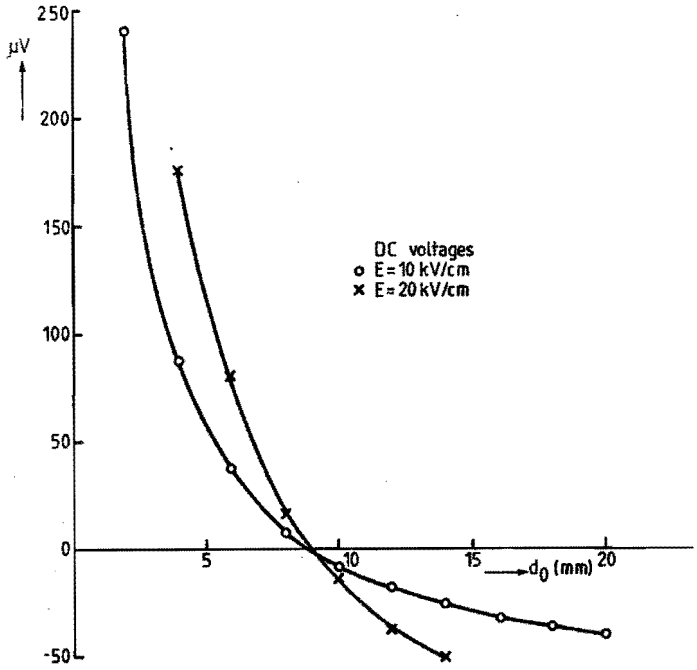

Figure 3.12 : Output voltage of the lock-in amplifier versus distance between hv electrode and measuring electrode for dc voltages.

The influence of the distance d_o between high voltage and measuring electrode is shown in Figure 3.12 of dc voltages and in Figure 3.13 for ac voltages. The two curves in each figure are measured for different field strengths.

The curves show in addition to the expected 1/d-like behavior a constant negative output which causes the signal to go through zero. This can be tentatively explained if the transducer does not vibrate in the axial direction only , but also in the radial direction. This effect is interesting because it gives a possibility for a field meter; it counteracts the effect of the "$\Delta\psi$"-current according to (3.11).

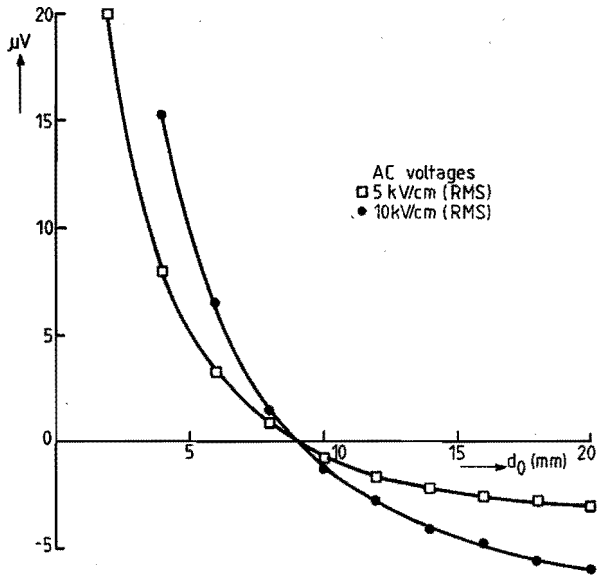

Figure 3.13 : Output voltage of the lock-in amplifier versus distance between hv electrode and measuring electrode for ac voltages.

These effects clearly cannot be separated with this transducer. To inhibit the vibration in the radial direction a new test set-up has been designed, see Figure 3.14; also here a commercially available transducer (Philips HPA) has been used. This set-up has two advantages:

- the amplitude of the vibration is larger: 20 μm,
- the elongation of the moving part gives a movement in the axial direction only.

The main disadvantage of the HPA is the low operating frequency, 5 kHz, which is in the audible range.

Due to a number of experimental difficulties no extensive measurements have been carried out up till now.

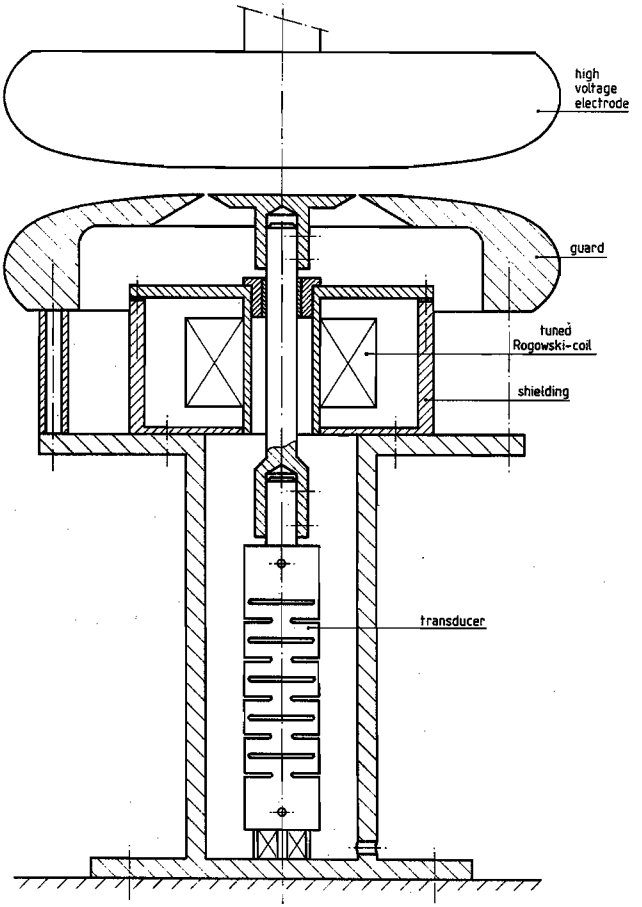

Figure 3.14 : Proposed test set-up with the HPA-transducer.

Another possibility to eliminate the radial vibration is to cover the edges of the Sonair transducer (i.e. to recess the transducer and extend the guard ring). The effect of the "$\Delta\psi$" current can be further increased by the use of a metal gauze, which would effectively increase the length of the dividing line between the stationary and the vibrating electrode.

4. WIDE BAND DETECTION OF PARTIAL DISCHARGES IN HIGH VOLTAGE CABLES

4.1. Introduction

This chapter describes a method for wide band detection of partial discharges in high voltage cables.
A partial discharge is defined as an electrical discharge which bridges the insulation between conductors only partially. When an insulating material is stressed electrically partial discharges may occur in gas filled cavities in the material, cavities which cannot be completely avoided during the manufacturing process. The partial discharges may give rise to a progressive deterioration of the insulation and eventually to a complete breakdown. The detection of partial discharges has therefore become a routine procedure for acceptance testing of power cables, switchgear, transformers etc.

In a partial discharge electrons and ions flow during a short time (less than 1 μs) whereas simultaneously acoustic, optical and radio frequent energy is emitted. An electrical measurement of the current flow caused by the discharge is a practical measuring method for a power cable. A wide band measurement offers the following advantages:
- the detection sensitivity can be increased,
- in cables transit time measurements are possible which means that a localization of the discharge site is feasible,
- the actual shape of the pulse from the discharge in the void can be studied.

In this chapter first attention is paid to an equivalent circuit for a partial discharge. Then the attenuation of the rf signals in the cable is treated. In the following sections several detection methods are discussed and the chapter ends with a number of experimental results among which oscillograms of actual pd signals are shown.

4.2. Theory

4.2.1. Equivalent circuits for a partial discharge

The description of the electrical phenomena related to partial discharges is usually based on the equivalent circuit of Figure 4.1 [Kr 64]. Capacitor c is the capacitance of the void, a is the capacitance of the sample and b is the capacitance of the dielectric between the electrodes and the void, in fact b consists of two capacitors in series. The spark gap symbolizes the breakdown of the cavity.

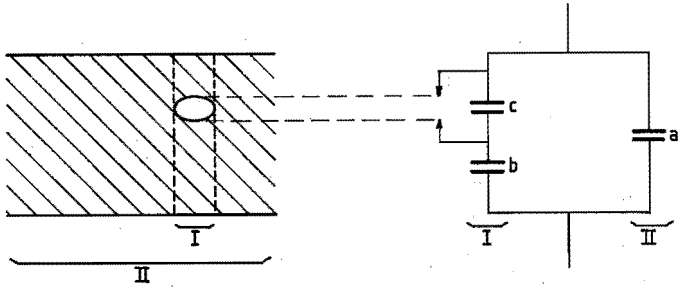

Figure 4.1 : Equivalent circuit for a partial discharge.

This model does not give a representation of the actual physical mechanism of a partial discharge and cannot explain the different waveforms of the current pulses, reported in the literature [Kä 76, Lu 79]. Furthermore, the essential effects of transit times and the dissipation cannot be described by the simple equivalent circuit of Figure 4.1 [Wo 81].

The equivalent circuit can be modified to include specific waveforms of the discharge current: the spark gap of Figure 4.1 is then replaced by a voltage source which delivers a pulse of the appropriate waveform.
Another problem with the equivalent circuit is the precise definition of the capacitor b. The capacitance of b depends on the

shape of the void, the distance to the electrodes and the discharge process, which can change the surface resistivity of the "electrodes" of capacitor b. This fact can be indicated in the equivalent circuit if b is taken to be a function of time: $b = b(t)$.

If the test sample is a high voltage cable, longer than a few meters, the transit time of the wave in the axial direction begins to exceed the pulse length. This means that capacitor a in Figure 4.1 has to be replaced by the characteristic impedance of the cable in each direction. The thus modified equivalent circuit is given in Figure 4.2.

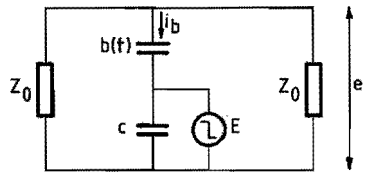

Figure 4.2 : Modified equivalent circuit for a partial discharge in a long cable.

We can derive the following equations for the amplitude of the travelling wave, e, and the apparent charge q, according to its usual definition:

$$i_b = \frac{d}{dt}\,(b(E-e)) \simeq \frac{d}{dt}\,(bE) \tag{4.1}$$

$$e = -\frac{Z_o}{2}\, i_b \tag{4.2}$$

$$q = \int_o^{T_o} i_b\, dt = -\frac{2}{Z_o} \int_o^{T_o} e\, dt = (bE)\,\Big|_{t=0} - (bE)\,\Big|_{t=T_o} \tag{4.3}$$

where T_o is the length of the discharge pulse and where $e \ll E$.

This means that the measurement of e provides information on the discharge process and measurement of the time integral of e gives the apparent charge.

4.2.2. Propagation of the pulses in the high voltage cable

In the preceding section the assumption was implicitly made, that the high voltage cable acts as an ideal coaxial cable, with no losses. Such a cable can be characterized by a simple and real wave impedance Z_o. However, a high voltage cable deviates in a number of aspects from this ideal coaxial cable:

- the skin effect in conductor and sheath is not negligible,
- the sheath is not a continuous cylinder but consists of copper wires spiralling around the insulation,
- the insulation is surrounded by extruded semiconducting layers (see page 48), both on the inside and the outside.

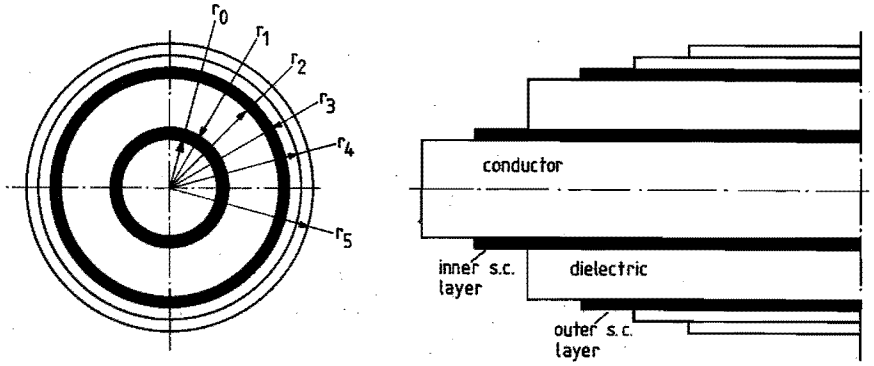

Figure 4.3 : Cross section of a 30/50 kV XLPE insulated cable.

Figure 4.3 gives the cross-section of a 30/50 kV XLPE[1)] insulated cable. Several models have been developed in the literature for the propagation of hf signals in high-voltage cables.

1) XLPE is an abbreviation for cross-linked polyethene.

These models are not only relevant for small partial discharge signals, but also for high voltage pulses, caused by lightning and switching surges. In the last case the attenuation can lead to a very desirable reduction of the overvoltages at the end of the cable.

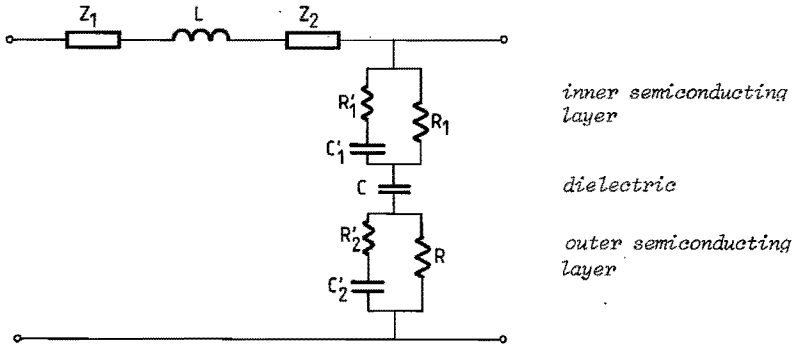

Figure 4.4 : Element of the transmission line equivalent circuit of a high voltage cable.

All these models use a long line model with a series impedance (Z) and a parallel admittance (Y) per unit length [Br 71, Du 78, St 82]. The series impedance, see Figure 4.4, is composed of the cable's inductance plus the skin-impedance of the inner and the outer conductors (the outer conductor is considered to be a hollow cylinder):

$$Z = Z_1 + j\omega L + Z_2 \tag{4.4}$$

where

$$L = \frac{\mu_o}{2\pi} \ln \left(\frac{r_3}{r_o}\right) \tag{4.5}$$

$$Z_1 = \frac{m_1}{2\pi r_o \sigma_1} \frac{I_o(m_1 r_o)}{I_1(m_1 r_o)} \tag{4.6}$$

$$Z_2 = \frac{m_2}{2\pi r_3 \sigma_2} \cdot \frac{I_o(m_2 r_3)\ K_1(m_2 r_4) + I_1(m_2 r_4)\ K_o(m_2 r_3)}{I_1(m_2 r_4)\ K_1(m_2 r_3) - I_1(m_2 r_3)\ K_1(m_2 r_4)} \qquad (4.7)$$

$$m_1 = \sqrt{(j\omega\mu_o\sigma_1)} = \frac{1+j}{\delta_1}\ ,\ m_2 = \sqrt{(j\omega\mu_o\sigma_2)} = \frac{1+j}{\delta_2}$$

The constants σ_1 and σ_2 are the conductivity, δ_1 and δ_2 the skin-depths of the inner and outer conductor respectively. The functions $I_o(x)$, $I_1(x)$, $K_o(x)$ and $K_1(x)$ are modified Bessel functions of the first and second kind and of zero and first order respectively. If the argument of such a function is much greater than unity (radius much greater than the skin-depth), it may be approximated by the first term of its asymptotic series. After some algebra this leads to:

$$Z_1 = \frac{1}{2\pi r_o} \sqrt{\left(\frac{j\omega\mu_o}{\sigma_1}\right)} \qquad (4.8)$$

$$Z_2 = \frac{1}{2\pi r_3} \sqrt{\left(\frac{j\omega\mu_o}{\sigma_2}\right)}\ \coth \sqrt{(j\omega\mu_o\sigma_2)}\, d \simeq$$

$$\simeq \frac{1}{2\pi b} \sqrt{\left(\frac{j\omega\mu_o}{\sigma_2}\right)} \qquad (4.9)$$

where d is the thickness of the outer sheath, $d = r_3 - r_o$. A model which includes the effect of separate neutral wires is given in [Du 78]; this model also includes the effects of the return currents in a nearby grounded plane. The semiconducting layers do not play a significant role in the series impedance Z: the current in the axial direction flows almost entirely through the central conductor and the sheath, because the conductivity of the s.c. layers is several orders of magnitude lower than the conductivity of the metal conductors.

The semiconducting layers are, however, important in the parallel admittance Y shown in Figure 4.4. The displacement current in the radial direction goes through the s.c. layers and the resistivity of these layers can cause extra losses. Therefore the admittance Y is given by the series combination of the

capacitance C (the conductance of the insulation can be neglected) and the admittances of the two s.c. layers:

$$Y = \frac{j\omega C\, Y_s}{Y_s + j\omega C}, \quad Y_s = \frac{Y_1\, Y_2}{Y_1 + Y_2} \tag{4.10}$$

The inner s.c. layer is only an extruded layer of polyethene with added carbon; the outer s.c. layer is composed of extruded conducting polyethene and two wrapped layers of carbon crepe paper.
A possible model for the electric behavior of the s.c. layer is given in Figure 4.4. The resistor R, the dc resistance of the material, is parallelled by a capacitance C' and a resistance R', simulating the ac impedance of the material. This gives the following general expression for the admittances Y_1 and Y_2 in (4.10):

$$Y = \frac{1 + j\omega(R+R')\, C'}{R(1 + j\omega R'C')} \tag{4.11}$$

The value of R can be determined from the measurement of the dc resistance in the axial direction.
The exact values of R' and C' cannot be measured; the s.c. layers are extruded simultaneously with the cable insulation and a mechanical separation is practically impossible.

However, the order of magnitude of C' (> 800 pF/m for the cable of Figure 4.3) results in a high impedance, compared with the resistance R (< 0.1 ohm) for frequencies to 200 MHz. The parallel branch can therefore be neglected in the first approximation which means that the impedance of the s.c. layer is purely resistive.

The attenuation α and the phaseshift β of the signals per meter cable length can now be calculated from

$$\alpha + j\beta = \sqrt{ZY} \tag{4.12}$$

where Z is defined in (4.4) and Y in (4.10). The attenuation α

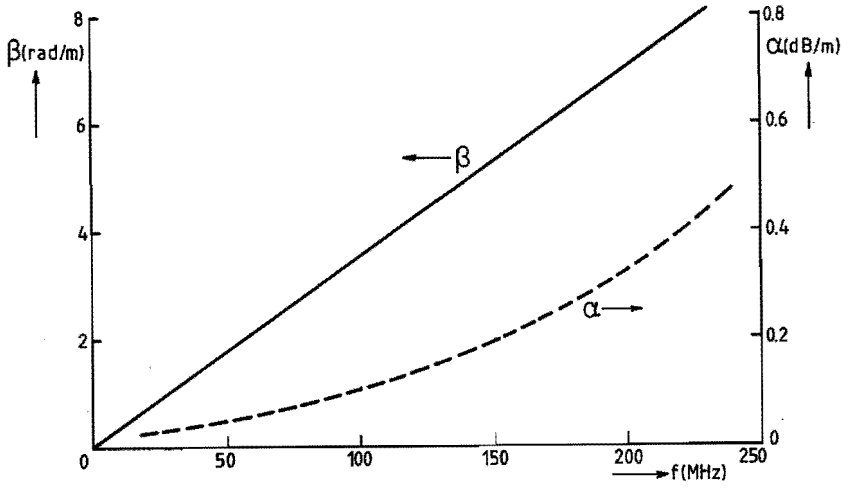

Figure 4.5 : The calculated attenuation α and phase shift β per meter length as a function of frequency for the 30/50 kV cable of Figure 4.3.

is expressed in Np/m (multiplication by 20 $^{10}\log$ e gives dB/m), the phaseshift β is expressed in radians/m. Generally α and β are frequency dependent, because Z and Y depend on the frequency. Figure 4.5 gives the calculated α and β for the 30/50 kV XLPE cable shown in Figure 4.3 as a function of frequency. The phaseshift β increases linearly with the frequency, which means that the group velocity v is constant according to:

$$\beta = \frac{\omega}{v} \qquad (4.13)$$

The experimental values of α and β will be reported in section 4.3.1.

4.2.3. Detection of the travelling waves

The travelling waves, generated by a partial discharge can be detected by several methods. Three detection methods (external capacitor, coaxial coupler and sheath interruption) are treated

in section 4.3.2. In this section a fourth detection principle will be briefly described.

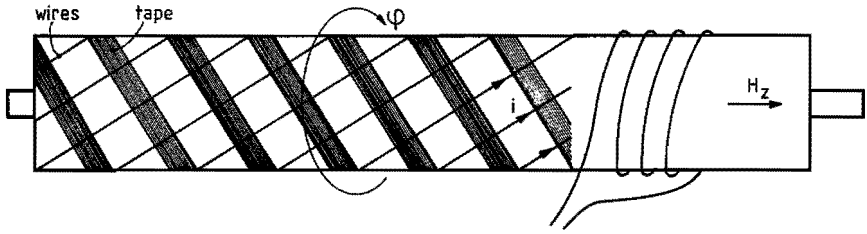

Figure 4.6 : Earth screen of the 30/50 kV cable with the measuring coil.

Most XLPE insulated cables in the voltage range up to 50 kV do not have a lead or aluminum sheath but have an earth screen of spiralled copper wire and a copper tape running in the opposite direction. The spiralling of the wires causes a current in the ϕ-direction (see Figure 4.6) which in turn causes a magnetic field in the axial direction, H_z. This field can be detected with a simple coil, a number of turns wound around the cable. If the amplitude of the travelling wave is e, the discharge current in the earth screen (and conductor) is given by:

$$i = \frac{e}{Z_o} = \tfrac{1}{2}\, i_b \qquad (4.14)$$

If the assumption is made that this current flows only through the spiralling wires, the magnetic field is given by:

$$H_z = \frac{i}{h} \qquad (4.15)$$

where h is the pitch of the neutral wires, see Figure 4.7. The measuring coil has N turns, the induced voltage V_{ind} is then given by:

$$V_{ind} = N \frac{d\Phi}{dt} = N \frac{d}{dt} \left(\frac{\mu_o \pi}{h} (r_3^2 - r_o^2)\, i\right) \qquad (4.16)$$

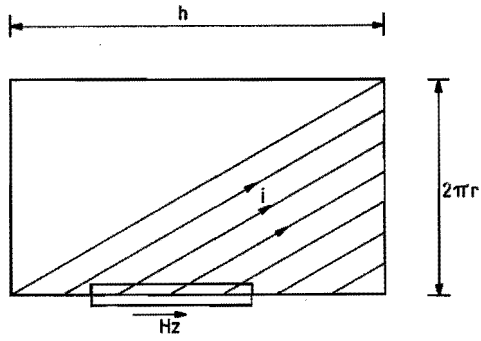

Figure 4.7 : Definition of the pitch (h) of the neutral wires.

From (4.2), (4.14) and (4.16) the relationship between V_{ind} and the discharge magnitude can be calculated:

$$V_{ind} = N \frac{\mu_o \pi}{2h} (r_3^2 - r_o^2) \frac{di_b}{dt} \qquad (4.17)$$

An integration of this induction voltage would give a signal proportional to i_b (compare (4.2)) which can be readily compared to partial discharge signals obtained by other methods, for instance the sheath interruption method.

The effect of the current in the spiralling wires is counteracted by a current in the oppositely wound copper tape. How the discharge current is shared between the wires and the tape depends on the respective selfinductances, on the mutual inductance between the wires and the tape and on the contact resistance. Especially the uncertainty about the contact resistance between wires and tapes makes it difficult to predict the sensitivity of the measuring coil. The described detection coil would have a number of advantages: no damage to the cable and directional sensitivity. No extensive experiments have been carried out up till now, due to the above mentioned difficulties.

4.2.4. The sensitivity of wide band discharge detection

The sensitivity of discharge detection usually refers to the smallest partial discharge (in pC) that can be detected. For narrow band detection systems the sensitivity for large objects is in the order of 0.1 pC under favorable conditions. For the calculation of the sensitivity in a wideband detection system the theory of optimum detection systems, developed for radar systems is useful [Bo 82].

The cable and the pd detection system can be considered as linear transfer systems, see Figure 4.8. The transfer function of the cable is derived in section 4.2.1. The transfer function of the detection system can be chosen as to match the signals from the cable.

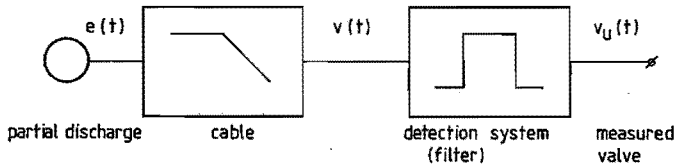

Figure 4.8 : Signal path from partial discharge to measured value. The cable and the detection system are considered as transfer systems.

A partial discharge generates a voltage pulse e between conductor and sheath of the cable, according to (4.2). The frequency-dependent attenuation of the cable changes the signal to v(t). If the detection system is ideal, the sensitivity is determined by the minimum permissible signal-to-noise (power) ratio, ρ:

$$\rho = \frac{E}{S_N} \tag{4.18}$$

where E is the energy of the pd pulse:

$$E = \frac{1}{Z_o} \int_{-\infty}^{\infty} v^2(t)\, dt \qquad (4.19)$$

and S_N is the noise power per Hz bandwidth [Wa 62]. Equation (4.18) is only valid when a so-called matched-filter is used for detection: a filter with a frequency dependent pass band matched to the incoming signal. Since a matched filter is difficult to realize, it is more convenient to use a rectangular bandpass-filter. The ratio ρ_R/ρ_M, where ρ_R and ρ_M are the S/N ratios for the rectangular and matched filters respectively, can be calculated [Wa 62] and is given in Figure 4.9 for a rectangular pulse of pulselength T (see Figure 4.10a) as a function of X, the product of T and the bandwidth $\Delta\omega$ of the filter:

$$X = \frac{\Delta\omega T}{2} = \pi\, \Delta f\, T \qquad (4.20)$$

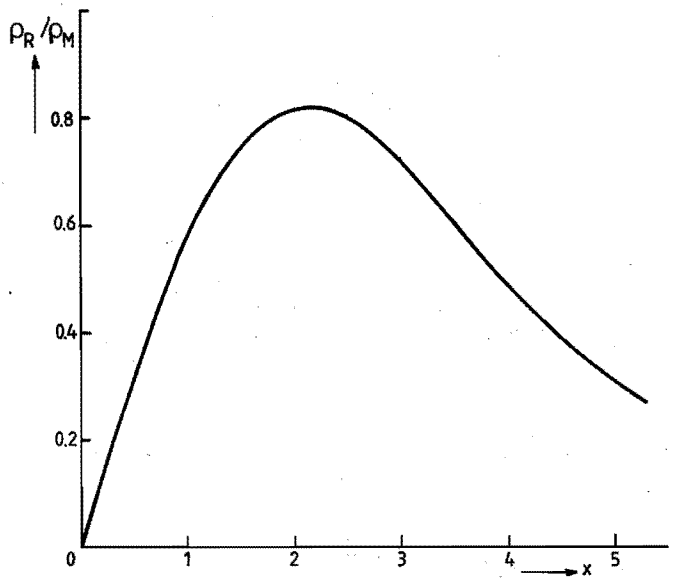

Figure 4.9 : Comparison of the rectangular bandpass filter (S/N ratio ρ_R) with the matched filter (S/N ratio ρ_M) for a rectangular input pulse of length T. On the horizontal axis the product of bandwidth and pulse length X = $\Delta\omega T/2$.

Figure 4.9 shows that the optimum bandwidth is reached when $X \simeq 2.15$, i.e. when

$$\Delta\omega = \frac{4.3}{T} \tag{4.21}$$

The value of ρ_R/ρ_M is then 0.825, i.e. 1.7 dB less than unity. This means that a rectangular bandpass filter is a good approximation for a matched filter and that equation (4.18) can be used to evaluate the detection sensitivity.

For the calculation of the energy E in the signal according to (4.19) the signal v(t) has to be known. This leads to rather tedious calculations because v(t) has to be found from the Fourier transform $V(\omega)$. A more simple approach is the direct calculation of E from $V(\omega)$ with the help of Parseval's formula [Pa 62]:

$$\int_{-\infty}^{\infty} v^2(t)\, dt = \frac{1}{2\pi} \int_{-\infty}^{\infty} |V(\omega)|^2\, d\omega \tag{4.22}$$

But how does the spectrum $V(\omega)$ look like for different types of discharge pulses and different cables?
The transfer function of the cable is calculated in section 4.2.1 and is given by:

$$H(\omega) = \exp\{-(\alpha+j\beta)l\} \tag{4.23}$$

α and β depend on the frequency; for simplicity we assume $\alpha = a\omega$, then $|H(\omega)|$ becomes:

$$|H(\omega)| = \exp(-a\omega l) \tag{4.24}$$

Also for simplicity a rectangular pulse e(t) with length T is assumed (Figure 4.10a), the spectrum $F(\omega)$ then becomes [Pa 62]:

$$F(\omega) = T\, \frac{\sin \frac{\omega T}{2}}{\frac{\omega T}{2}} \tag{4.25}$$

see Figure 4.10b.

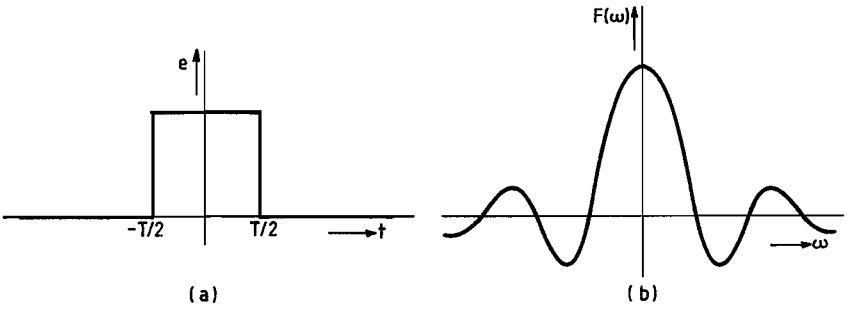

Figure 4.10 : Shape of the input pulse e(t) (a) and corresponding spectrum F(ω) (b).

From (4.24) and (4.25) the spectrum V(ω) can be calculated:

$$|V(\omega)| = T \frac{\sin \frac{\omega T}{2}}{\frac{\omega T}{2}} e^{-a\omega l} \qquad (4.26)$$

The phase shift of the signals is ignored in (4.26). Figure 4.11 gives a picture of $|V(f)|$ for different values of the pulse length T. A cable length of 30 m and a value for a of $2.5 * 10^{-9}$ dB/Hz.m was assumed, corresponding to Figure 4.15. The only influence of the rectangular bandpass characteristic of the detection system is a limitation of the spectrum to $\pm \Delta\omega$.

From (4.19), (4.22) and (4.26) the energy of the signal after passing the cable can be calculated as a function of the pulse length T. The result is given in Figure 4.12. The reference is the energy of the original signal (not attenuated by the cable) with the same amplitude. Especially short pulses are strongly attenuated by the cable.
The preceding calculations and Figure 4.12 provide sufficient information to calculate the minimum detectable partial discharge. The available thermal noise power per Hz bandwidth at 290 K is given by:

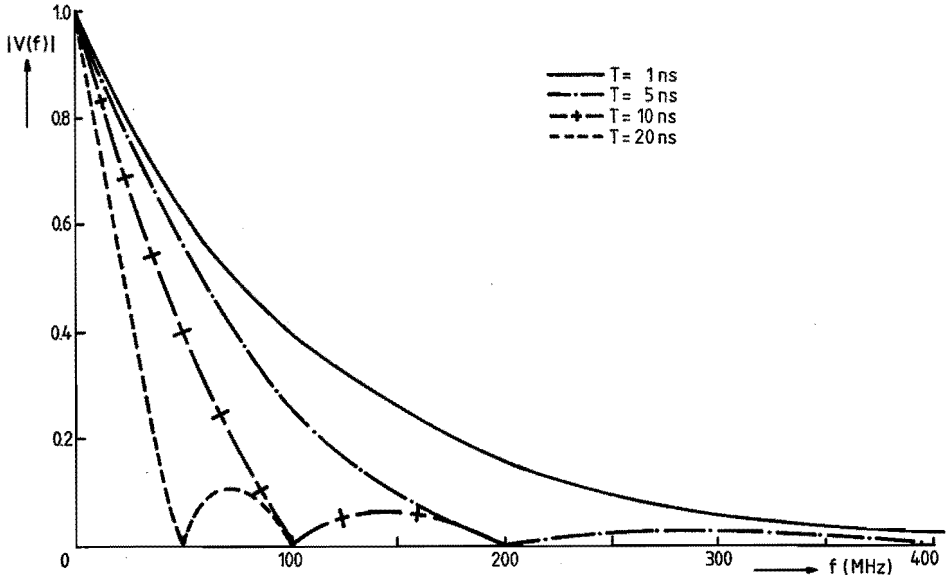

Figure 4.11 : Spectrum V(f) for rectangular pulses of various pulse widths, after attenuation by 30 meters the of 30/50 XLPE cable under consideration.

$$S_N = kT = 4 * 10^{-21} \text{ W/Hz} \qquad (4.27)$$

Although a S/N ratio of 0 dB is acceptable when the discharges are displayed on a CRT the losses of the detection system (coupling losses) and the extra noise of the amplifiers have to be taken into account. The coupling losses can be as high as 10 dB ([Bo 82], see also section 4.3.2), while a practical wide band amplifier adds 5 - 10 dB noise. Therefore the minimum acceptable S/N ratio is set to 20 dB here. This leads to a minimum signal energy of $4 * 10^{-19}$ J.

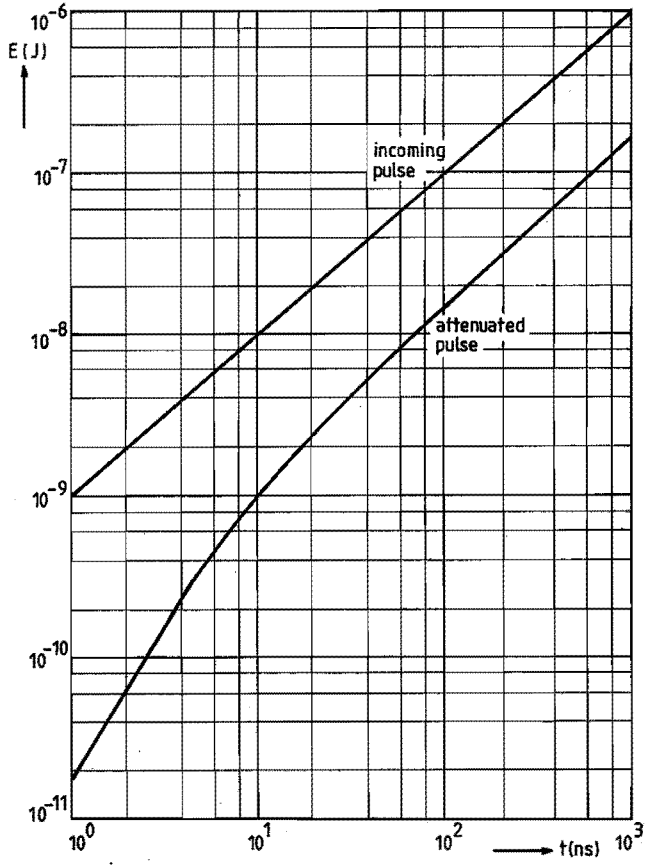

Figure 4.12 : Energy content of the original and the attenuated partial discharge pulse as a function of the pulse width. The amplitude of the incoming pulse is 1 Volt (across 34 Ω), the pulse width T.

With Figure 4.12 and equations (4.2) and (4.3) the minimum detectable signal can be calculated in terms of charge. The results are given in Figure 4.13. The lower curve gives the sensitivity in the case of no attenuation, the upper curve gives the values with the attenuation present. The sensitivity (for this type and length of cable!) is clearly limited to 0.05 pC.

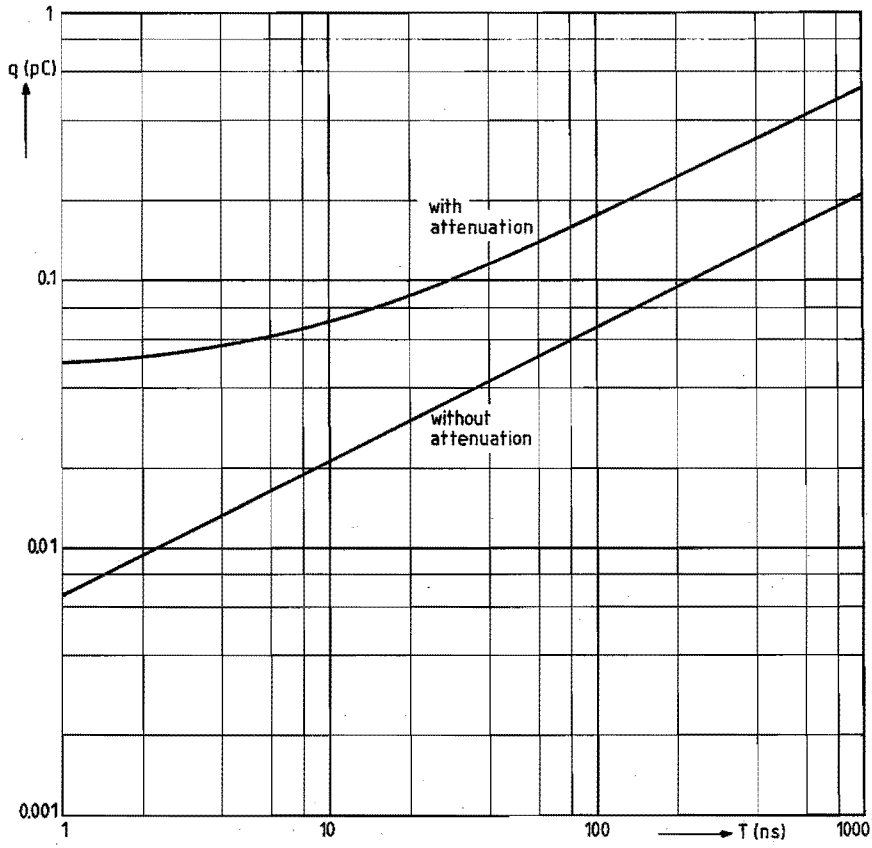

Figure 4.13 : The smallest detectable partial discharge vs pulse length for 30 meter of the XLPE cable under consideration.

The Figures 4.11 and 4.13 also give an indication for the optimum bandwidth of the detection system. Equation (4.21) gives for a 1 ns pulse a bandwidth of 680 MHz, while Figure 4.11 shows, that the spectrum is falling rapidly above 300 MHz. Also Figure 4.13 confirms that the cable itself limits the propagation of very short pulses rather than the detection system.

The practical situation can deviate from the preceding theory on two important points:

- the pulse form of an actual pd is usually not rectangular. However, the results with other pulse forms will not differ much from the results obtained here, see e.g. [Bo 82].
- the different locations of discharge sites result in different distances to the detection point. As the attenuation is a function of distance, the same pd signals at different sites have different spectra upon detection. This fact can hardly be accounted for in theory.

To conclude this section some remarks should be made about further enhancement of the S/N ratio. The application of correlation techniques to pd measurements was first reported by Wilson [Wi 73]. The primary technique is signal averaging, although auto- and cross-correlating can also be used [Be 71]. However, there are a number of problems involved in signal averaging:

- a partial discharge is a random process [Be 71]; the averaging can only be successful if the repeatability of the discharge in each cycle is sufficiently high.
- The repetition rate of the pd signals is 50 Hz. The enhancement of the S/N ratio is proportional to the number of repetitions [Tr 68]. This means for a 20 dB improvement already a measuring time of 2 s.
- The situation gets worse for a wideband detector. The limited time resolution of a multichannel averager requires the use of a boxcar averager here. A boxcar averager is in fact a single channel averager, which only takes one sample per period. This elongates the measuring time by an order of magnitude [Wi 73].

These problems make it clear that signal correlation techniques cannot really improve the S/N ratio in pd measurements significantly.

4.3. Experiments

4.3.1. Measurements on the propagation of hf signals in power cables

The attenuation and phase shift of hf signals were measured on the 30/50 kV cable shown in Figure 4.3. The cable is terminated with its characteristic impedance (34 Ω), composed of 10 discrete low inductance resistors in parallel. The measurements were carried out with a HP 8405A vector voltmeter and a HP 8654A RF generator; the experimental set-up is given in Figure 4.14.

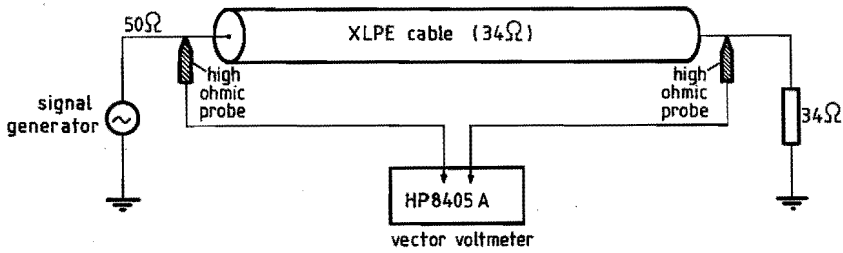

Figure 4.14 : Test set-up for the attenuation measurements.

The transition in characteristic impedance from the 50 Ω of the signal generator cable to the 34 Ω of the XLPE cable gives rise to a reflection of about 17% of the signal. This does not influence the measurements because both incoming and outgoing signals are measured with high impedance (100 kΩ, 2.5 pF) probes. The attenuation per meter cable length as a function of frequency is given in Figure 4.15. The measured values are significantly higher than the values calculated in Section 4.2.2. This can be due to the fact that the properties of the s.c. layers were unsufficiently known. The measured attenuation of $2.5 * 10^{-9}$ dB/m.Hz happens to be in good agreement with the value measured by Stone and Boggs [St 82] for a similar type of cable.

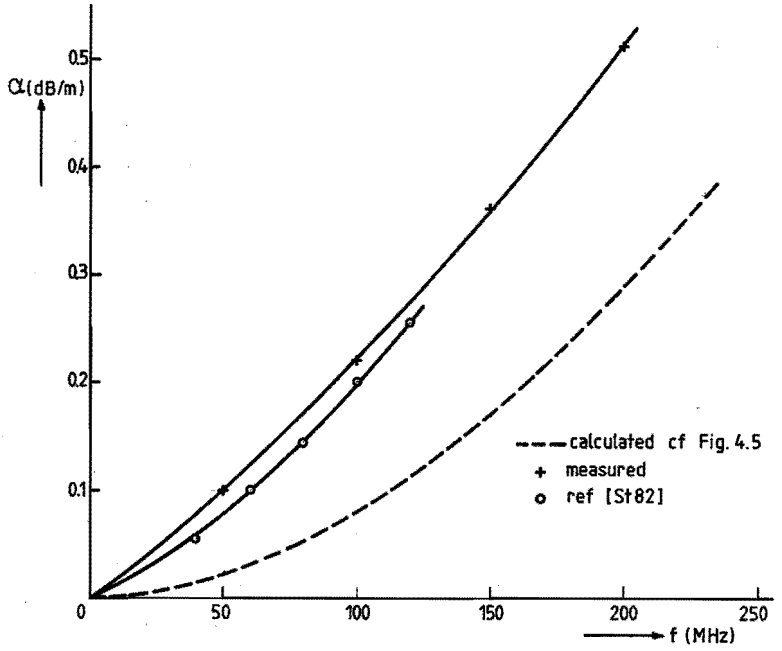

Figure 4.15 : The attenuation per meter cable length as a function of frequency.

The phase shift per meter cable length is given in Figure 4.16 as a function of frequency. The difference between the calculated and the measured value is much smaller here; if the group velocity is calculated with (4.13) a value of $v = 1.9 * 10^8$ m/s is found. This is in good agreement with the value that has been determined by transit time measurements.

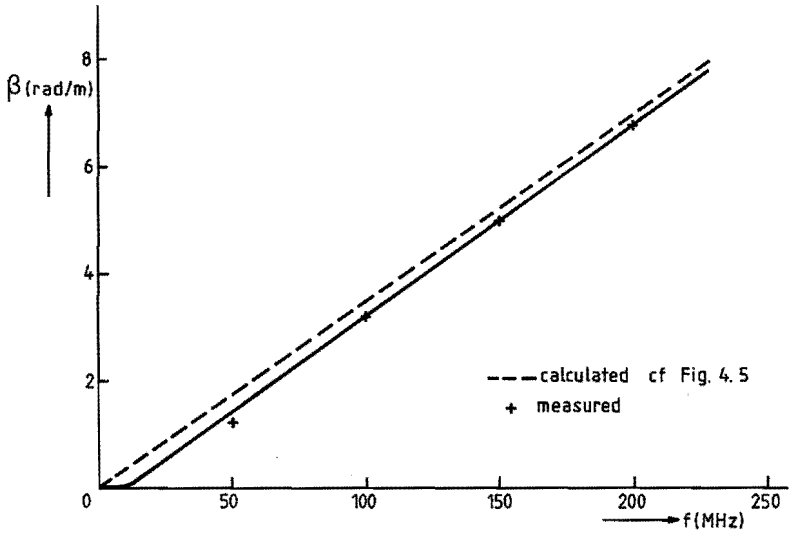

Figure 4.16 : Phase shift per meter cable length as a function of frequency.

FOURTH
INTERNATIONAL SYMPOSIUM
ON HIGH VOLTAGE ENGINEERING
ATHENS - GREECE, 5 - 9 SEPTEMBER 1983

63.02

WIDE BAND DETECTION OF PARTIAL DISCHARGES IN HIGH VOLTAGE CABLES

G.G. Wolzak
Eindhoven University of Technology
Department of Electrical Engineering
Eindhoven, The Netherlands

Abstract

Wide band detection of partial discharges offers several advantages over the more classical narrow band method. Especially in distributed systems with relatively low losses (like GITL) which permit a bandwidth of up to 1 GHz the sensitivity can be increased by an order of magnitude. An additional advantage is the possibility of localization of the discharge sites.
We have developed some improvements on the wide band detection method, applied for cables of short length. Experiments with low-loss coaxial cables show the increased detection sensitivity and the accurate localization.
In high voltage solid dielectric cable the losses - caused probably by the semi-conducting extruded layers - are higher and frequency dependent. This sets a limit to the maximum usable bandwidth. A careful layout of the measuring circuit and numerous shielding measures allowed a detection sensitivity of 0.1 pC. The localization of the discharge sites was possible with an accuracy of ± 20 cm.

Keywords

Partial discharge, cable, localization.

1. Introduction

Partial discharges have a limiting effect on the life time of many high voltage constructions. Therefore the measurement of partial discharges (pd) has become a routine procedure for acceptance testing of power cables, transformers, switchgear etc.
The improved production technology of solid dielectric cables causes the magnitude of pd in the cables to decrease, which calls for a more sensitive detection system.
There are two methods for pd detection in cables: the classical narrow band method and the wide band method The latter was mainly developed for the localization of discharge sites in long (> 500 m) cables. Recently a systematic study was reported [1] on the improvement of detection sensitivity that can be obtained by the wide band method, both for Gas Insulated Transmission Line (GITL) and solid dielectric cable.
As a part of a larger project which has to establish the role of very small pd on the life expectancy of solid dielectric cable we had to develope some improvements on the wide band detection method, applied for cables of short length (30 m). These improvements should enable us to detect partial discharges of less then 0.5 pC and localize then with an accuracy of 0.5 m; analysis of the pulse shape should also be possible.

2. Wide band detection methods.

A pd in the insulation of a cable generates travelling waves which propagate in two directions along the cable. With the widely adopted equivalent circuit of Figure 1 we can calculate the relationship between the amplitude of these travelling waves and the discharge current or the apparent charge [2] . We can derive:

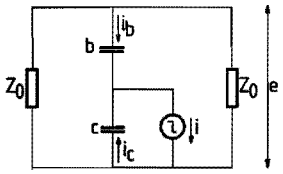

Figure 1. Equivalent circuit for a pd in a long cable.

$$e = \frac{Z_o}{2} i \qquad (1)$$

$$q = \int_o^{T_o} i_b = -\frac{2}{Z_o} \int_o^{T_o} e.dt \qquad (2)$$

where T_o is the length of the discharge pulse. The voltage e gives information on the discharge current, the integral on the apparent charge q. The travelling waves can be detected in three ways:
1. In the external circuit with a coupling capacitor and a detection impedance. This method is described recently by Lemke [3] and Beyer [4]. There are a number of disadvantages to this method:
- the coupling capacitor which should have a value of 1-10 nF and should be discharge free tends to be very expensive for voltages above 100 kV,
- the physical size of the coupling capacitor and its leads limits the frequency response of the input circuit at high frequencies,
- localization is obtained by the measurement of the time difference of the incident and the reflected signal. The attenuation of the signal limits the applicability of this method for very small pd. Reeves [5] has tried to overcome this difficulty by using two capacitors and a dual beam oscilloscope for very accurate localization.

2. Boggs and Stone [1] describe the use of coaxial coupling capacitors built into GITL; this input circuit shows an excellent hf behavior. However, an analogous coupling capacitor in solid dielectric cable requires two complete sheath interruptions.
3. The travelling waves can be detected with a measuring resistor across an interruption of the cable sheath. This method was originally reported by Kreuger [2] but has received little attention since. The advantages are:
- no external coupling capacitor is needed,
- the coaxial geometry of the cable is disturbed,
- a sheath interruption near each end of the cable gives the possibility of localization irrespective of signals, reflected at the ends of the cable.

We have adopted this last method for the detection of small pd in short cables.

3. Description of the measuring method.

3.1. Theory.

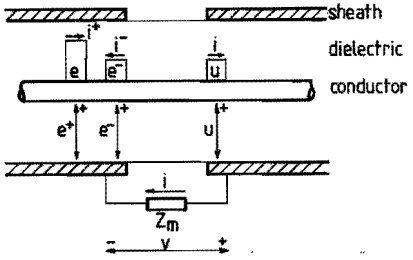

Figure 2. Signals at a sheath interruption.

A picture of incident, reflected and transmitted signals at an interruption of the cable sheath is given in Figure 2. Important for pd detection is the relationship between the voltage across the measuring impedance Z_m and the original wave amplitude e:

$$v = 2e \cdot \frac{Z_m}{Z_m + 2Z_o} \qquad (3)$$

The measuring impedance Z_m can be formed by a discrete resistor, the resistance of a semiconducting layer or the input impedance of the measuring system.

In the more refined equivalent circuit of Figure 3 we have included the 'ground-impedance' Z_g, the wave impedance of the cable sheath with respect to the nearby ground plane.

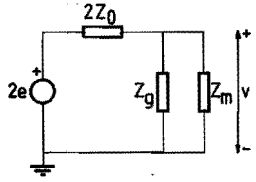

Figure 3. Equivalent circuit of sheath interruption.

With this change (3) turns into:

$$v = 2e \cdot \frac{Z_m}{Z_m + 2Z_o \left(1 + \frac{Z_m}{Z_g}\right)} \qquad (4)$$

3.2. Measuring circuits.

With two sheath interruptions in a cable, one at each end, the following detection circuits are possible:

- straight detection at one interruption can be used for analysis of the pd pulse shape. For localization one of the two following circuits has to be used.
- detection with two interruptions in parallel, see Figure 4a. The equivalent circuit is given in Figure 4b.
- balanced detection, see Figure 4c. The measuring cable with characteristic impedance Z_m is connected between a. en b. A balun (balanced-unbalanced transformer) has to be used to match the differential voltage $v_a - v_b$ to the asymmetric measuring cable and oscilloscope amplifier

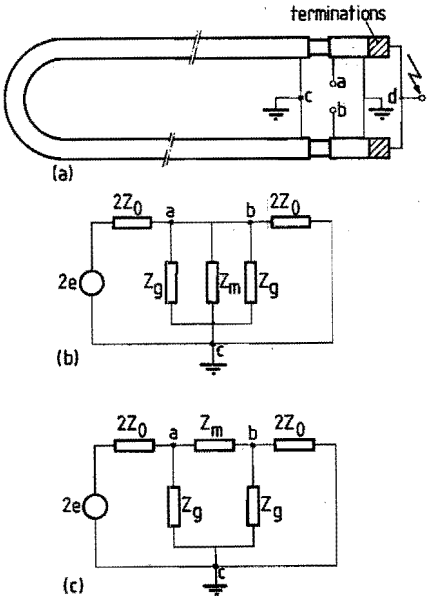

Figure 4. Possible measuring circuits:
(a) cable and sheath interruptions
(b) unbalanced detection, equivalent circuit
(c) balanced detection, equivalent circuit
The two voltage sources in (b) and (c) represent the incident wave fronts which may arrive at different moments.

The balanced circuit can be used for the suppression of external interference. However, this advantage is only fully exploited when the remaining cable lengths beyond the interruptions are equal and the high voltage connection (point d. in Figure 4.a) is located halfway the two terminations; only then the transit times of the interfering signals to the interruptions are equal so that they do not show up in $v_a - v_b$.

3.3. Localization.

Localization of a discharge site in the cable between the interruptions is possible by the measurement of the time difference of the pulses, arriving at the interruptions. In two cases this procedure can give some difficulties:

- a pd located exactly in the middle of the cable does not register in the balanced dectection set-up, because the two signals arrive at the interruptions simultaneously. The best solution to this problem is to measure with two signals and a dual beam oscilloscope or with the balanced setup.
- a discharge site in the immediate vicinity of a sheath interruption leads to more complicated signals because reflections from the terminations arrive quickly. In the interpretation one should note that the polarity of the measured pulses depends on the direction in which the wave propagates.

The length of the cable between the interruptions can easily be determined by the injection of a simulated discharge pulse at one interruption which is then measured at both interruptions. The reflected signals from the terminations should not interfere with the direct signals. This can be achieved when the sheath interruptions are at a sufficiently large distance from the terminations. A length of 2 to 3 meters cable is enough.

4. Apparatus.

All measurements were carried out in the shielded high voltage laboratory of the Eindhoven University of Technology. The excellent shielding of this laboratory gives a 80 dB damping of unwanted signals.

For the pd measurement we used a Tektronix 7844 dual beam oscilloscope with a bandwidth of 400 MHz. The oscilloscope was placed in a small shielded measuring cabin. The measuring cable (RG 214 U) is laid in a copper pipe. The characteristic impedance of this terminated cable forms the input impedance of the measuring system.
Measurement of very small pd is possible by the use of Avantek pre-amplifiers. We used two types, with bandwidths of 2 MHz - 550 MHz and 200 Hz - 550 MHz. The gain of both types was 28 dB and their noise 53 μV_{eff}. The smallest detectable signal was therefore 150 μV_{pp}.
Several types of balun were used, constructed according to [6]. All had a small ferrite toroidal core, with 7 to 13 turns of wire on it.

5. Experiments.

5.1. Tests with RG 214 U and RG 218 U cables.

These cables, with a characteristic impedance $Z_o = 50\Omega$ were used for calibration and initial tests. Simulated discharge pulses were injected into a cable with no terminations; from the signals measured at the interruptions we were able to calculate the ground impedance Z_g.
For this cable and interruptions, Z_g was about 200Ω. The very small damping of the cables causes little attenuation or distortion of the pd signals. Therefore we were able to measure very small discharges and locate them very accurately. Figure 5 gives a picture of a pd in a RG 214 U cable. The discharge magnitude was 0.44 pC and the detection circuit of Figure 4.b was used.

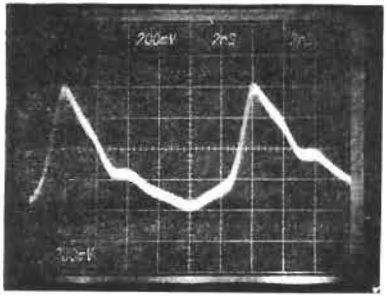

Figure 5. Partial discharge in a RG 214 U cable.

The length of the cable was 20 m; the localization of the discharge site was possible with an accuracy of ± 3 cm.
The smallest pd we have observed in this cable was 0.04 pC, with a pulse duration of 5 ns. With (2) and (4) we can calculate, that this is just above the theoretical minimum (0.03 pC) for the given pulse length.

5.3. Tests with 30/50 kV XLPE cables.

These power cables have a characteristic impedance of about 34Ω. Sheath interruptions are made in the copper wires of the ground shield. The outer semiconductive layer then gives a measuring resistance of 500 to 1000Ω, parallel to the 50Ω input impedance of the measuring system.
A number of tests with simulated discharge pulses showed these cables to have a rather high attenuation of hf signals. This can probably be attributed to the semiconductive layers [7]. The detailed results of the attenuation measurements and calculations will be reported in the near future.

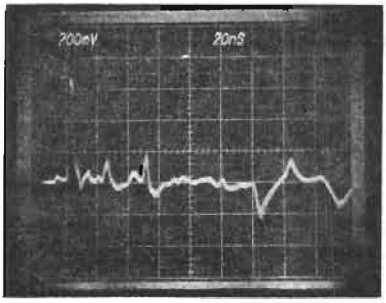

Figure 6. Partial discharge in a 30/50 kV XLPE cable.

A typical example of a pd in the XLPE cable is given in Figure 6. Signals of this kind are difficult to integrate for the measurement of the apparent charge q. We therefore have used a conventional ERA-3 detector for reference measurements.
The smallest discharge we have observed in the power cables was a 0.4 pC, 10 ns pulse. This discharge could be localized with an accuracy of ± 20 cm.

6. Conclusion.

The experiments have shown that wide band detection of partial discharges is possible in short high voltage cables with solid dielectric. The losses in the extruded inner and outer semiconductive layers limit the maximum usable bandwidth to about 100 MHz.
A number of shielding precautions can bring down the measuring sensitivity to less than 0.5 pC.
Wide band detection makes localization of discharge sites possible. In the paper this was done by oscilloscope measurements, but the use of more advanced electronics is possible.

7. Acknowledgement.

The author thanks prof. P.C.T. van der Laan for his constant interest and encouragement. He acknowledges the help of E.F. Steennis in an earlier part of the work.
The measuring method was developed as a part of a research contract with KEMA, The Netherlands.

8. References.

[1] Boggs, S.A., Stone, G.C.: "Fundamental limitations in the measurement of corona and partial discharge". IEE Transactions vol EI 17 (1982) pp 143-150.
[2] Kreuger, F.H.: "Discharge detection in high voltage equipment". Heywood, London, 1964.
[3] Lemke, E.: "A new method for pd measurement on polyethylene insulated power cables". 3rd International Symposium on High Voltage Engineering, Milan, Italy, 28-31 August 1979, Paper 43.13.

[4] Beyer, M., Borsi, H., Feser, K., Kamm, W.: "A new method for detection and location of geometrically distributed partial discharges (cable faults) in high voltage cables under external interference".
CIGRE SC 15 Colloquium Liège, Belgium, 24 August 1981.

[5] Reeves, J.H.: "The location of partial discharge sites in h.v. switchgear and short cables by a travelling wave method".
CIRED, Brighton, UK, 1-5 June 1981, paper 4.12

[6] Ruthroff, C.L.: "Some broad-band transformers". Proceedings of the IRE, vol 47 (1959) pp. 1337-1342.

[7] Stone, G.C., Boggs, S.A.: "Propagation of partial discharge pulses in shielded power cable".
CEIDP, Amherst, 17-21 October 1982, pp. 275-280.

REFERENCES

[Be 63] Bewley, L.V.
TWO-DIMENSIONAL FIELDS IN ELECTRICAL ENGINEERING.
New York: Dover, 1963. Reprint of the 1948 ed.

[Be 71] Bendat, J.S. and A.G. Piersol
RANDOM DATA: Analysis and measurement procedures.
New York: Wiley, 1971.

[Bo 82] Boggs, S.A. and G.C. Stone
FUNDAMENTAL LIMITATIONS IN THE MEASUREMENT OF CORONA AND PARTIAL DISCHARGES.
IEEE Trans. Electr. Insul., Vol. EI-17(1982), p. 143-150.

[Br 71] Breien, O. and I. Johansen
ATTENUATION OF TRAVELLING WAVES IN SINGLE-PHASE HIGH-VOLTAGE CABLES.
Proc. Inst. Electr. Eng., Vol. 118(1971), p. 787-793.

[Ca 75] Carlson, A.B.
COMMUNICATION SYSTEMS: An introduction to signals and noise in electrical communication. 2nd ed.
New York: McGraw-Hill, 1975.
McGraw-Hill electrical and electronic engineering series

[Du 78] Dugan, R.C. and W.L. Sponsler
SURGE PROTECTION OF UD CABLE SYSTEMS. Part 2: Analytical models and simulations.
IEEE Trans. Power Appar. & Syst., Vol. PAS-97(1978), p. 1901-1909.

[Go 40] Gohlke, W. und U. Neubert
BEMERKUNGEN ZUR HOCH- UND HÖCHSTSPANNUNGSMESSUNG.
Z. Tech. Phys., Vol. 21(1940), p. 217-222.

[Gr 69] Groenenboom, M. en H.A.J.M. Spoorenberg
DE ESPOM: Een capacitief gekoppelde elektronische spanningstransformator.
Smit Meded., Vol. 24(1969), p. 223-232.

[IE 79] CONVENTIONAL AND UNCONVENTIAL CURRENT AND VOLTAGE TRANSFORMERS WITH PARTICULAR REFERENCE TO USE WITH SOLID STATE DEVICES. Proc. Coll., London, 26 Jan. 1979.
London: Institution of Electrical Engineers, 1979.
IEE Colloquia Digest No. 1979/7.

[Kä 76] Kärkkäinen, S.
INTERNAL PARTIAL DISCHARGES: Pulse distributions, physical mechanisms and effects on insulations.
Ph.D. Thesis. Helsinki University of Technology, 1976.
Espoo: Technical Research Centre of Finland, 1976.
Electrical and nuclear technology publication, 14.

[Ke 64] Keller, R.
WIDEBAND HIGH VOLTAGE PROBE.
Rev. Sci. Instrum., Vol. 35(1964), p. 1057-1060.

[Kr 64] Kreuger, F.H.
DISCHARGE DETECTION IN HIGH VOLTAGE EQUIPMENT.
London: Heywood, 1964.

[Lu 79] Luczyński, B.
PARTIAL DISCHARGES IN ARTIFICIAL GAS-FILLED CAVITIES IN SOLID HIGH VOLTAGE INSULATION.
Ph.D. Thesis. Technical University of Denmark (Lyngby), 1979.
Electric Power Engineering Department, Publication No. 7902.

[Ni 63] Nie, A.G. van and J.J. Zaalberg van Zelst
A VIBRATING CAPACITOR DRIVEN BY A HIGH-FREQUENCY ELECTRIC FIELD.
Philips Tech. Rev., Vol. 25(1963/64), p. 95-103. Dutch version: Philips Tech. Tijdschr., Vol. 25(1963), p. 77-85.

[Pa 62] Papoulis, A.
THE FOURIER INTEGRAL AND ITS APPLICATIONS.
New York: McGraw-Hill, 1962.
McGraw-Hill electronic sciences series

[Pr 69] Prinz, H.
HOCHSPANNUNGSFELDER.
München: Oldenbourg, 1969.

[St 82] Stone, G.C. and S.A. Boggs
PROPAGATION OF PARTIAL DISCHARGE PULSES IN SHIELDED POWER CABLE.
In: Annual Report 51st Conf. on Electrical Insulation and Dielectric Phenomena, Amherst, Mass., 17-21 Oct. 1982.
Piscataway, N.J.: IEEE Service Center, 1982. P. 275-280.

[To 82] Tokoro, K. et al.
DEVELOPMENT OF ELECTRONIC POTENTIAL AND CURRENT TRANSDUCERS SUITABLE FOR GAS INSULATED SWITCHGEAR AND ADEQUATE FOR APPLICATION TO SUBSTATION DIGITAL CONTROL SYSTEMS.
IEEE Trans. Power Appar. & Syst., Vol. PAS-101(1982), p. 3967-3976.

[Tr 68] Trimble, C.R.
WHAT IS SIGNAL AVERAGING?
Hewlett-Packard J., Vol. 19, No. 9(April 1968), p. 2-7.

[Wa 62] Wainstein, L.A. and V.D. Zubakov
EXTRACTION OF SIGNALS FROM NOISE.
Englewood Cliffs, N.J.: Prentice-Hall, 1962.
Translated from Russian.

[Wo 81] Wolzak, G.G. and P.C.T. van der Laan
DISCUSSION ON THE EQUIVALENT CIRCUIT OF A PARTIAL DISCHARGE: Possible new measurement techniques.
Paper presented at the Coll. of the CIGRE Study Committe 15 (Insulating Materials) on the Detection and Effects of Partial Discharges in Insulating Materials, Liège, 24 Sept. 1981. Abstracts in: Electra (Paris), No. 80(Jan. 1982), p. 43-45. Full text obtainable from the authors: Department of Electrical Engineering, Eindhoven University of Technology, Netherlands.

[Zi 32] Zisman, W.A.
A NEW METHOD OF MEASURING CONTACT POTENTIAL DIFFERENCES IN METALS.
Rev. Sci. Instrum., Vol. 3(1932), p. 367-370.

SAMENVATTING

Dit proefschrift beschrijft de ontwikkeling van enige meetmethoden op het gebied van de hoogspanningstechniek. Hierbij ligt het accent op meetmethoden voor hoge spanning en op detectiemethoden voor partiële ontladingen.
Voor het meten van hoge spanningen zijn twee methoden ontwikkeld, beide met als ingangscircuit een enkele hoogspanningscondensator.

De eerste methode wordt beschreven in hoofdstuk 2 en is gebaseerd op achtereenvolgende differentiatie en integratie van het signaal. Een belangrijk voordeel van deze methode is, dat tussen hoogspanningsdeel en meetinstrument een lange coaxiale meetkabel gebruikt kan worden. Deze karakteristiek afgesloten meetkabel vormt dan een integraal deel van het meetsysteem. Op basis van dit principe zijn verschillende uitvoeringen gerealiseerd voor het meten van gelijk-, wissel- en stootspanningen; de resultaten van de metingen met deze apparaten worden ook in hoofdstuk 2 beschreven.

De tweede methode van spanningsmeting is een moderne uitvoering van de generererende voltmeter. In hoofdstuk 3 wordt een voltmeter beschreven die geen roterende maar een vibrerende meetelektrode heeft, aangedreven door een piëzo-elektrische transducer. In het kort worden de mogelijkheden aangegeven dit apparaat te gebruiken voor het meten van spanningen en elektrische velden. Tevens wordt een beschrijving gegeven van de benodigde apparatuur om het gemoduleerde signaal van de bewegende elektrode om te zetten in een spanning die evenredig is met de te meten spanning.

De detectie van partiële ontladingen in hoogspanningskabels is het onderwerp van hoofdstuk 4. Door een partiële ontlading, veroorzaakt door een holte in het diëlektricum van de kabel ontstaan lopende golven tussen geleider en mantel. Na een kort overzicht van de vervangingsschema's voor een partiële ontlading wordt de voortplanting van deze golven langs de kabel nader bestudeerd. De verzwakking van de lopende golven wordt voornamelijk veroorzaakt door de halfgeleidende schermen (geleider- en aderscherm)

aan weerszijden van de isolatie. Het theoretische model hiervoor wordt door middel van verzwakkingsmetingen geverifieerd. Gegeven deze eigenschappen van de kabel is de kleinst detekteerbare partiële ontlading bepaald met behulp van een theoretisch model. Voor 30 m kabel van een bepaald type (30/50 kV XLPE) blijkt deze kleinste ontlading 0.05 pC te zijn.
De lopende golven kunnen op twee manieren worden gedetecteerd: door middel van een onderbreking van de kabelmantel óf met behulp van een spoeltje dat om de kabel gewonden is. De tweede methode wordt hier slechts kort beschreven.
Het hoofdstuk eindigt met enige experimentele resultaten, waaronder oscillogrammen van enige kleine partiële ontladingen in verschillende typen kabel.

DANKBETUIGING

Het in dit proefschrift beschreven onderzoek werd uitgevoerd in het Hoogspanningslaboratorium van de vakgroep "Technieken van de Energievoorziening" van de TH Eindhoven.
Velen, in en buiten deze vakgroep, hebben hierbij hun medewerking gegeven.
Prof.dr.ir. P.C.T. van der Laan ben ik erkentelijk voor zijn voortdurende interesse in en stimulering van het onderzoek.
Herrn Prof. Dr.-Ing. K. Möller danke ich für die bereitwillige Übername des zweiten Referates und die rasche Durchsicht des Manuskriptes.
De technische staf van het hoogspanningslaboratorium ben ik dank verschuldigd voor de steun bij de experimentele realisatie van het onderzoek. Zonder de overige leden te kort te doen wil ik op deze plaats met name mijn "technische rechterhand" Th.G.M. van Moorsel vermelden.
Zonder de financiële en materiële steun van de N.V. KEMA te Arnhem, NKF Kabel B.V. te Delft en COQ B.V. te Amersfoort zou het onderzoek op deze schaal niet mogelijk geweest zijn.
Een belangrijke bijdrage aan het onderzoek werd ook geleverd door mijn afstudeerders ir. J.A.G. Bekkers, ir. E.F. Steennis, ir. H.A. Minkman, ir. W.Chr. van Abkoude en E.J. Bresser. Hiervoor mijn dank, die tevens geldt voor de stagiairs die bij het onderzoek betrokken waren.
Mevr. W.M.L. Marrevée en mevr. T.J.F.M. Pellegrino typten de tekst voor dit proefschrift; F.M. van Gompel leverde niet alleen technische assistentie bij het onderzoek maar verzorgde ook het tekenwerk. Hen allen dank ik hartelijk.
Mevr. M.J. van Megen tenslotte wil ik bedanken voor het ontwerpen van de omslag.

LEVENSLOOP

Gerard Wolzak werd op 10 november 1952 geboren te Oosterbeek. In 1970 behaalde hij het diploma HBS-B aan het Nijmeegs Lyceum. Zijn ingenieursdiploma aan de Afdeling der Elektrotechniek van de Technische Hogeschool te Eindhoven behaalde hij in 1977. Het afstudeerwerk, een onderzoek naar de mogelijkheden voor ultrasonore verstuiving van cesium in een MHD-generator, verrichtte hij onder leiding van prof.dr. L.H.Th. Rietjens.
Vanaf mei 1977 tot september 1978 vervulde hij als vaandrig, werkzaam bij de Commissie van Proefneming van de Landmacht, zijn dienstplicht.
Vervolgens werkte hij van september 1978 tot november 1979 als research medewerker in het Hoogspannings Research Laboratorium van NKF Kabel B.V. te Delft.
Sinds november 1979 is hij werkzaam in het Hoogspanningslaboratorium van de Technische Hogeschool te Eindhoven, aanvankelijk als wetenschappelijk assistent, vanaf maart 1982 als wetenschappelijk ambtenaar. Zijn werk, onder leiding van prof.dr.ir. P.C.T. van der Laan, leidde tot dit proefschrift.

Stellingen

behorend bij het proefschrift van

G.G. Wolzak

1. Bij iedere meting in de hoogspanningstechniek is een correcte definitie van het - vaak omvangrijke en onoverzichtelijke - ingangscircuit van groot belang. Het onderscheid, dat Gallagher en Pearmain maken tussen "voltage pulse detection" en "current pulse detection" is een voorbeeld van onvolledig inzicht in de aard van het ingangscircuit.

   Dit proefschrift, hoofdstuk 1
   T.J. Gallagher, A.J. Pearmain,
   High voltage - measurement, testing and design
   (John Wiley, New York 1983)

2. Het door Bahder et.al. voorgestelde model voor de veroudering van kabels met kunststofisolatie onder invloed van het elektrische veld kan niet worden toegepast op moderne XLPE kabels met hoge bedrijfsveldsterkte.

   G. Bahder et.al., IEEE Transactions vol. PAS - 101 (1982) pp. 1379-1382.
   G. Bahder et.al., IEEE Transactions vol. PAS - 102 (1983) pp. 2173-2182.

3. Het uitwerken van een "whole vehicle radiated susceptibility test" aan een voertuig wordt bij hoge frequenties steeds moeilijker door het sterke richteffect van de antennes. In dit licht gezien is het frequentiebereik waarover een dergelijke test dient te worden uitgevoerd volgens SAE J 1338 (10 kHz - 18 GHz) niet realistisch.

   SAE Publication J 1338, in: SAE Handbook 1982 (Soc. of Automotive Eng., Warrendale, 1982).

4. Van de bestaande typen spanningsdelers biedt de differentierende/integrerende deler de beste mogelijkheid om als onderdeel van de deler een lange, karakteristiek afgesloten kabel naar het meetinstrument toe te passen.

   Dit proefschrift, hoofdstuk 2.

5. De optredende knik in de stijgende flank van een coronapuls, zoals deze is gemeten door Zentner, vindt zijn oorzaak in het meetsysteem en niet in een fundamenteel verschijnsel.

   R. Zentner, Zeitschr. angew. Physik 29 (1970) pp. 294-301.

6. Gezien de macromoleculaire structuur van polyetheen is het uitvoeren van een zgn. naaldtest aan dit materiaal te vergelijken met het prikken van een scherpgepunte wandelstok in een emmer, gevuld met rubber ballen. Op grond van de resultaten van dergelijke "naaldtests" kunnen derhalve geen uitspraken over intrinsieke materiaaleigenschappen worden gedaan.

7. Het model dat door Stone en Boggs wordt gebruikt voor de beschrijving van een halfgeleidende laag in een hoogspanningskabel geeft geen adequate beschrijving van de verzwakking van hoogfrequente signalen.

   G.C. Stone, S.A. Boggs, Conf. on El.Ins. and Diel. Phen., Amherst (1982) pp. 275-280.
   Dit proefschrift, hoofdstuk 4.

8. Om een objectieve voorlichting aan de deelnemers van het "Informatie en communicatie experiment Zuid-Limburg" te waarborgen, verdient het aanbeveling in dit gebied op ruime schaal Orwell's boek "1984" te verspreiden.

9. De door Nikolopoulos en Topalis aangegeven methode voor het corrigeren van fouten, veroorzaakt door stootspanningsmeetsystemen, kan onder ongunstige omstandigheden aanleiding geven tot grotere fouten in het gecorrigeerde dan in het oorspronkelijke signaal.

   P.N. Nikolopoulos, F. Topalis, Fourth Int.Symp. on High Voltage Eng., Athens (1983) paper 65.08
   B.R. Hunt, IEEE Transactions vol. AC 17 (1972) pp. 703-705.

10. De aanwezigheid van oppervlaktelading op een isolerende spacer beïnvloedt de doorslagspanning van het spacer-gas systeem. Het is niet correct - hoewel uit praktisch oogpunt begrijpelijk - dat deze oppervlaktelading vaak na het wegnemen van het elektrische veld gemeten wordt.

    L.G. Christophorou (ed.), Gaseous Dielectrics III, chapter 8 (Pergamon Press, New York, 1982).

11. De slechte economische situatie in de bouw biedt een goede gelegenheid de sterk versnipperde structuur - die voor een belangrijk deel verantwoordelijk is voor de geringe technische vooruitgang in deze bedrijfstak - te veranderen.

12. De uitvinding van het "scratchen" in de discomuziek dient te worden gezien als een oneigenlijk middel tot het stimuleren van de platen verkoop en niet als het toevoegen van een nieuw element in deze muziek.